Eur. J. Mech. B - Fluids 20 (2001) 699–726

S0997-7546(01)01154-2/FLA

A PDF propagation approach to model turbulent dispersion in swirling flows

J.S. Shirolkar [1], Mardson Q. McQuay *

Department of Mechanical Engineering, 435 CTB, Brigham Young University, Provo, UT 84602, USA

(Received 25 September 1999; revised 30 May 2001; accepted 4 June 2001)

Abstract – A computationally efficient approach that solves for the spatial covariance matrix along the dense particle ensemble-averaged trajectory has been successfully applied to describe turbulent dispersion in swirling flows. The procedure to solve for the spatial covariance matrix is based on turbulence isotropy assumption, and it is analogous to Taylor's approach for turbulent dispersion. Unlike stochastic dispersion models, this approach does not involve computing a large number of individual particle trajectories in order to adequately represent the particle phase; a few representative particle ensembles are sufficient to describe turbulent dispersion. The particle Lagrangian properties required in this method are based on a previous study (Shirolkar and McQuay, 1998). The fluid phase information available from practical turbulence models is sufficient to estimate the time and length scales in the model. In this study, two different turbulence models are used to solve for the fluid phase – the standard k–ε model, and a multiple-time-scale (MTS) model. The models developed here are evaluated with the experiments of Sommerfeld and Qiu (1991). A direct comparison between the dispersion model developed in this study and a stochastic dispersion model based on the eddy lifetime concept is also provided. Estimates for the Reynolds stresses required in the stochastic model are obtained from a set of second-order algebraic relations. The results presented in the study demonstrate the computational efficiency of the present dispersion modeling approach. The results also show that the MTS model provides improved single-phase results in comparison to the k–ε model. The particle statistics, which are computed based on the fundamentals of the present approach, compare favorably with the experimental data. Furthermore, these statistics closely compare to those obtained using a stochastic dispersion model. Finally, the results indicate that the particle predictions are relatively unaffected by whether the Reynolds stresses are based on algebraic relations or on the turbulence isotropy assumption.

turbulence / particle dispersion / swirling flows / Markovian approach

Nomenclature

A_{kq}	Any tensor	M	Transformation matrix
a_k	Any vector	P	Gaussian probability density function
C	Model constant	R	Normalized fluctuating velocity correlation
c_μ	Model constant	r	Radial distance
d	Diameter	Re	Reynolds number
d_t	Zero mean normal random variable	S	Source term
g	Gravitational acceleration	T	Surrounding fluid time scale in the absence of drift
k	Turbulent kinetic energy		
L	Integral length scale	t	Time
l	Characteristic length scale	$\vec{u}$	Velocity vector
m	Mass; Loop parameter in Frenkiel function	u	Axial velocity
$\dot{m}_p$	Particle mass flow rate	v	Radial velocity

* Correspondence and reprints.
E-mail address: mq01@byu.edu (M.Q. McQuay).
[1] Present address: MicroStrategy, Inc., 8000 Towers Crescent Drive, Vienna, VA 22182, USA.

v_d	Particle drift velocity
W	Weight function
w	Tangential velocity
z	Axial distance

Greek Symbols

β	Fluid integral length scale ratio
Δ	Difference
Δt	Time increment
ε	Dissipation rate of turbulent kinetic energy
μ	Dynamic viscosity
ν	Kinematic viscosity
ϕ	General transported property
Φ	Production term
ρ	Density
ρ_c	Correlation coefficient
σ	Standard deviation; Model constant
σ_{ij}	Particle spatial covariance matrix
η	Ensemble mean particle location
θ	Angle of rotation
$\dot{\theta}$	Rate of rotation
γ	Model constant
Γ	Diffusion coefficient
τ	Time scale
τ_p	Particle relaxation time
$\langle\ \rangle$	Ensemble mean quantity

Subscripts

11 and 22	Transverse directions
33	Longitudinal direction
E	Eulerian
e	Relative to an eddy
f	Fluid phase
i	ith coordinate direction
ii	Tensor with $i = j$
ij	Tensor
j	jth coordinate direction
L	Lagrangian
p	Particle phase; Pertaining to production range
r	Pertaining to radial distance
sf	Pertaining to fluid surrounding a heavy particle
t	Turbulent; Pertaining to dissipation range
z	Pertaining to axial distance
ϕ	Pertaining to the ϕ transported property

Superscripts

L	Lagrangian
N	New coordinate system
ϕ	Pertaining to the ϕ transported property
$'$	Fluctuations
—	Time average

1. Introduction

The current effort in turbulent dispersion modeling focuses on developing reliable and efficient methods based on turbulence models applicable to practical systems. Studies have shown that the stochastic dispersion models which rely on a Monte Carlo procedure to represent the particle phase require about 2000 to 6000 individual particle trajectory calculations per particle size to correctly predict dispersion in isotropic, homogeneous decaying turbulent flows (Milojevic [1]; Lu [2]). Recently, a new approach to model turbulent dispersion of heavy particles has been developed based on Taylor's theory (Taylor [3]) and the particle momentum equation (Shirolkar and McQuay [4]). In this model, the spatial spread (variance) for a group of particles is computed along the particle ensemble mean trajectory. This model, when evaluated with the aid of experiments of Snyder and Lumley [5] and Wells and Stock [6], showed that one particle ensemble calculation per particle size can provide excellent predictions for particle dispersion and particle velocity decay

in isotropic, homogeneous decaying turbulence. Thus, the computational advantage of this approach is obvious in simple flows. It has also been shown that this approach gives better overall particle predictions in isotropic, homogeneous turbulence in comparison to certain stochastic models commonly used today (Shirolkar and McQuay [4]). The objective of the present paper is to extend this concept, which is referred to as the Probability Density Function Propagation (PDFP) approach, to model a complex flow involving inhomogeneities, such as the case of swirling flows.

A large majority of particle dispersion models solve for individual particle trajectories (representing a certain particle mass flow rate) in a Lagrangian framework. They are commonly known as Stochastic-Separated-Flow (SSF) models because they treat the carrier phase and the particle phase separately. These models are stochastic in nature because they rely on computing a large number of particle trajectories (Monte Carlo method) in order to properly characterize the particle phase. These SSF models solve the particle equation of motion, determining how the particles travel in a given flow field. The turbulent dispersion is accounted for by estimating the instantaneous fluid velocity needed in the particle equation of motion. Based on the method used to estimate this fluid velocity, these models can be classified as (i) models based on the eddy lifetime concept (Gosman and Ioannides [7]; Shuen et al. [8]; Chen and Crowe [9]), and (ii) time-correlated dispersion models (Zhuang et al. [10]; Berlemont et al. [11]; Burry and Bergeles [12]; Lu et al. [13]; Chen and Pereira [14]). The eddy lifetime concept models sample the fluctuating part of the instantaneous fluid velocity from a known distribution and this fluid velocity is assumed to act on the particle for a duration known as eddy-particle interaction time. It is also assumed that the fluid velocities are independent of each other in successive interaction times. Such assumptions oversimplify the time correlations in the turbulent velocities (Shirolkar et al. [15]). The time-correlated models overcome the disadvantages of the eddy lifetime models by including a fluid particle trajectory that runs directly along the (dense) particle trajectory. The fluid particle trajectory is generated by using a Markov-chain model, which is capable of incorporating the time correlations in the fluid fluctuating velocity (Sawford [16]; Durbin [17]). In these models, the required fluid fluctuating velocity along the particle trajectory is then obtained with the aid of spatial correlation functions. The time-correlated models rely on sampling of a zero-mean normal random variable to account for uncertainties in turbulence (Shirolkar et al. [15]).

The SSF model based on the eddy lifetime concept is extensively used in two-phase flow predictions. In some situations, the number of particle trajectory calculations for monosized particles required in the SSF model for an invariant solution is as high as 9000 to 10 000 (Mostafa and Mongia [18]; Adeniji-Fashola and Chen [19]; Chen and Pereira [20]). In polydispersed flows, the required number of particle calculations is naturally greater (Chen and Pereira [20,21]). Furthermore, the number of particle calculations is also strongly depended on the nature of the coupling that exists between the particle and the fluid phase (Kohnen et al. [22]; Berlemont et al. [23]).

In an industrial application, such as pulverized-coal combustion systems, there is a great need to correctly account for particle dispersion, because the particle phase influences various processes like heat transfer, pollutant formation, and fouling and slagging inside the combustor. In such systems, the coupling between the dispersed phase and the carrier phase is quite strong. The particle spatial distribution determines the locations in which the particle burns as it exchanges mass, momentum, and energy with the carrier gas phase. Thus the particle dispersion phenomenon greatly influences the various gas phase properties such as velocity, temperature, and density. The above SSF models can be easily incorporated in a comprehensive, pulverized-coal combustion code. However, since these models rely on random sampling of certain distributions, they require a large number of trajectory computations in order to represent the particle phase adequately. A typical full-scale pulverized-coal combustor can require up to 10^6 trajectory computations (Coimbra et al. [24]), but, such large number of particle calculations are obviously economically impractical. In practice, limited

particle trajectories are computed instead of totally neglecting the dispersion phenomenon (see [24]). However, such practices have to devise special methods to ensure the overall convergence of the flow field which is threatened by the unsteady particle source terms introduced due to insufficient particle calculations (Shirolkar et al. [15]; Boyd and Kent [25]). In other pulverized-coal combustion codes, a modified-deterministic approach is used to account for the dispersed phase (Smoot et al. [26]). Although these modified-deterministic models are computationally efficient, the quality of predictions obtained from such models is poor (Shirolkar and Queiroz [27]).

The need to develop computationally effective dispersion models is apparent from the above discussion. In response to this need, some investigators have attempted to develop an efficient approach based on the original eddy lifetime concept of Gosman and Ioannides [7] (Litchford and Jeng [28]; Chen and Pereira [20]). In the approach of Litchford and Jeng [28] the main idea is to limit the sampling requirements in the eddy lifetime approach and, at the same time, to minimize the numerically induced noise. However, since this approach is based on the eddy lifetime concept, it inherits its previously discussed limitations. Furthermore, this approach also requires the Monte Carlo procedure to properly account for particle dispersion in nonhomogeneous turbulence.

An alternative to the SSF models is to develop a method directly based on Taylor's [3] theory on turbulent dispersion. Such a method would solve for the instantaneous spatial dispersion of particles as they move in the Lagrangian reference frame, and would thus preclude the need to generate large numbers of individual trajectories while at the same time correctly accounting for turbulent dispersion. Taylor's approach has been successfully applied to describe turbulent motion of fluid particles, but has had limited success in modeling dense particle dispersion. The reason for this lack of success is that the Lagrangian particle properties needed in Taylor's approach are difficult to obtain, either from experiments or from practical models. In the PDFP approach of Shirolkar and McQuay [4], the required Lagrangian particle properties are estimated from the particle momentum equations and the information available from turbulence models applicable to practical systems. The present study demonstrates how this approach can be extended to model turbulent particle dispersion in nonreacting, axisymmetric swirling flows. In the present study, the PDFP dispersion model is solved in conjunction with two different practical turbulence models: the standard k–ε model, and the MTS turbulence model. The evaluation of the PDFP model is done primarily with the help of the experimental data of Sommerfeld and Qiu [29]. Their experiments consist of detailed measurements of a swirling, particle-laden, two-phase flow, using a laser-based instrument. The PDFP model is also evaluated by comparing its predictions with a SSF model based on the eddy lifetime approach.

2. Description of the modeling approaches

The present study uses the standard k–ε model and the MTS model to solve the time-averaged, steady-state Navier–Stokes equations for an incompressible Newtonian fluid. The general form of these equations, which is applicable to an axisymmetric swirling flow, is the following partial differential equation:

$$\frac{\partial}{\partial z}(\bar{\rho}\bar{u}\phi) + \frac{1}{r}\frac{\partial}{\partial r}(r\bar{\rho}\bar{v}\phi) - \frac{\partial}{\partial z}\left(\Gamma_\phi \frac{\partial \phi}{\partial z}\right) - \frac{1}{r}\frac{\partial}{\partial r}\left(r\Gamma_\phi \frac{\partial \phi}{\partial r}\right) = S_\phi, \tag{1}$$

where ϕ is the transported property, $\bar{\rho}$ is the specific mass of the fluid, Γ_ϕ is the diffusion coefficient for the property ϕ, and S_ϕ is a source term. The property ϕassumes various values, such as 1 for continuity, $\bar{u}_i$ for momentum, k for turbulent kinetic energy, and ε for the rate of dissipation of the turbulent kinetic energy.

The standard k–ε model is a single time scale turbulence model; in other words, only one time scale represents both the turbulent transport of mass and momentum and the dissipation of the turbulent kinetic energy. According to Kim [30], using only one time scale rapidly degenerates the predictive capability of the k–ε model for complex flow situations, such as confined swirling flows. As a result, the program in this study was developed to provide the option of using a multiple-time-scale model for turbulence instead of the original k–ε model. The MTS model implemented here is the same one proposed by Kim and Chen [31,32] and it is based on a single-point closure and a simplified, split-spectrum method. In this model, the turbulent kinetic energy spectrum is partitioned into a production range (turbulent kinetic energy of the large eddies, or k_p) and a dissipation range (turbulent kinetic energy of the fine scale eddies, or k_t). In the method developed by Kim and Chen [32], the partitioning of the kinetic energy spectrum is variable, and the location of the partition is determined as part of the solution. The MTS model uses four partial differential equations for turbulence closure in order to account for production, cascade, and dissipation of turbulent kinetic energy. These are: (i) the turbulent kinetic energy of large eddies, k_p; (ii) the turbulent kinetic energy of fine scale eddies, k_t; (iii) the energy transfer rate from large scale to fine scale eddies, ε_p; and (iv) the dissipation rate of the turbulent kinetic energy, ε_t.

The fluid phase partial differential equations needed to solve for nonreacting, axisymmetric swirling flows, using both the $k-\varepsilon$ and the MTS models for closure, are summarized in *table I*. This table also shows the respective model constants that will be used in the present study. The total kinetic energy of the turbulence, k, as solved by the $k-\varepsilon$ model is equivalent to the sum of the kinetic energies of the large scale and fine scale eddies in the MTS model ($k_p + k_t$). Also, the two dissipation rates, ε and ε_t, model the same physical phenomenon.

The fluid phase equations are solved in a staggered, nonuniform, orthogonal grid in which the coefficients are calculated by a line-by-line, full-elliptic, Tri-Diagonal Matrix Algorithm (TDMA). A consistently formulated QUICK scheme proposed by Hayase et al. [33] is employed to discretize the convective term in the control-volume formulation. Also, a third-order boundary treatment is used for cells adjacent to the walls ([33]).

The momentum exchange between the fluid phase and the particle phase is accounted for by calculating the appropriate source terms and adding them to the respective fluid phase momentum equations (see S_p^{ϕ} in *table I*). The overall calculation procedure consists of the following steps: (i) set up the initial and boundary conditions for the given problem; (ii) partially converge the fluid phase equations; (iii) calculate the particle statistics/trajectories based on the dispersion model; (iv) calculate the momentum sources for each cell in the computational domain; (v) add the respective momentum source terms in the governing fluid phase equations and partially converge them; and (vi) repeat steps (iv) and (v) until overall convergence is achieved.

As indicated earlier, this paper evaluates the PDFP model for turbulent dispersion, using experimental data for particle dispersion in a swirling flow (Sommerfeld and Qiu [29]). Shown below is a detailed description of the present effort to model the problem of particle dispersion in axisymmetric swirling flows, assuming turbulence isotropy. This model is also evaluated by comparing its predictions with a standard Lagrangian dispersion model based on the eddy lifetime concept. A brief description on the eddy lifetime concept model used here is also provided below.

2.1. The PDF propagation model for turbulent dispersion

The PDFP model used in this study is the one proposed by Shirolkar and McQuay [4]. In general, the model solves for the particle ensemble mean position and spatial variances in turbulent flows. The ensembles mean trajectories are based on the solution of the ensemble-averaged particle momentum equations, while the particle positional variances are calculated by assuming turbulence isotropy. The PSI-CELL technique of Crowe et al. [34] is used to account for momentum exchange between the two phases. The particle source terms for a

Table I. The fluid phase equations for k–ε and MTS models.

$$\frac{\partial}{\partial}(\bar{\rho}\bar{u}\phi) + \frac{1}{r}\frac{\partial}{\partial r}(r\bar{\rho}\bar{v}\phi) - \frac{\partial}{\partial z}\left(\Gamma_\phi \frac{\partial \phi}{\partial z}\right) - \frac{1}{r}\frac{\partial}{\partial r}\left(r\Gamma_\phi \frac{\partial \phi}{\partial r}\right) = S_\phi$$

ϕ	Γ_ϕ	S_ϕ
1	0	0
$\bar{u}$	μ_e	$-\frac{\partial \bar{p}}{\partial z} + \frac{\partial}{\partial z}\left(\mu_e \frac{\partial \bar{u}}{\partial z}\right) + \frac{1}{r}\frac{\partial}{\partial r}\left(r\mu_e \frac{\partial \bar{v}}{\partial z}\right) + S_p^u$
$\bar{v}$	μ_e	$-\frac{\partial \bar{p}}{\partial r} + \frac{\partial}{\partial z}\left(\mu_e \frac{\partial \bar{u}}{\partial r}\right) + \frac{1}{r}\frac{\partial}{\partial r}\left(r\mu_e \frac{\partial \bar{v}}{\partial r}\right) - 2\mu\frac{\bar{v}}{r^2} + \frac{\bar{\rho}\overline{w}^2}{r} + S_p^v$
$\overline{w}$	μ_e	$-\frac{\bar{\rho}\bar{v}\,\overline{w}}{r} - \frac{\overline{w}}{r^2}\frac{\partial}{\partial r}(r\mu_e) + S_p^w$
k–ε Model		
k	μ_e/σ_k	$\Phi - \bar{\rho}\varepsilon$
ε	μ_e/σ_ε	$\frac{\varepsilon}{k}[C_{\varepsilon 1}\Phi - C_{\varepsilon 2}\bar{\rho}\varepsilon]$
MTS Model		
k_p	μ_e/σ_{kp}	$\Phi - \bar{\rho}\varepsilon_p$
k_t	μ_e/σ_{kt}	$\bar{\rho}(\varepsilon_p - \varepsilon_t)$
ε_p	$\mu_e/\sigma_{\varepsilon p}$	$C_{p1}\frac{\Phi^2}{\bar{\rho}k_p} + C_{p2}\frac{\Phi\varepsilon_p}{k_p} - C_{p3}\frac{\bar{\rho}\varepsilon_p^2}{k_p}$
ε_t	$\mu_e/\sigma_{\varepsilon t}$	$C_{t1}\frac{\bar{\rho}\varepsilon_p^2}{k_t} + C_{t2}\frac{\bar{\rho}\varepsilon_p\varepsilon_t}{k_t} - C_{t3}\frac{\bar{\rho}\varepsilon_t^2}{k_t}$

where $\Phi = \mu_\varepsilon\left\{2\left[\left(\frac{\partial \bar{u}}{\partial z}\right)^2 + \left(\frac{\partial \bar{v}}{\partial r}\right)^2 + \left(\frac{\bar{v}}{r}\right)^2\right] + \left[\frac{\partial \bar{u}}{\partial r} + \frac{\partial \bar{v}}{\partial z}\right]^2 + \left[r\frac{\partial}{\partial r}\left(\frac{\overline{w}}{r}\right)\right]^2 + \left(\frac{\partial \overline{w}}{\partial z}\right)^2\right\}$

$\mu_e = \mu_{\text{laminar}} + \mu_{\text{turbulent}}$

Model constants

k–ε model: $C_\mu = 0.09$; $C_{\varepsilon 1} = 1.44$; $C_{\varepsilon 2} = 1.92$

$\sigma_k = 1.0$; $\sigma_\varepsilon = 1.30$; $\sigma_t = 0.7$

$\mu_{\text{turbulent}}(\mu_t) = C_\mu \bar{\rho}\frac{k^2}{\varepsilon}$

MTS model: $C_\mu = 0.09$; $C_{p1} = 0.21$; $C_{p2} = 1.24$; $C_{p3} = 1.84$

$C_{t1} = 0.29$; $C_{t2} = 1.28$; $C_{t3} = 1.66$

$\sigma_{kp} = 0.75$; $\sigma_{kt} = 0.75$; $\sigma_{\varepsilon p} = 1.15$; $\sigma_{\varepsilon t} = 1.15$; $\sigma_t = 0.7$

$\mu_{\text{turbulent}}(\mu_t) = C_\mu \bar{\rho}\frac{k^2}{\varepsilon_p}$; $k = k_p + k_t$

particular Eulerian cell are calculated from the predicted number of particles in that cell. The mathematical details are presented below.

In this model, the particles with similar physical properties and the same initial conditions are assumed to have a Gaussian distribution in space at any given time. This assumption makes it possible to track the positional Probability Density Function (PDF) of a group of particles rather than individual particle trajectories. For a two-dimensional problem, the expression for the joint normal positional PDF is given in terms of the ensemble mean particle location (η_i) and the corresponding particle ensemble covariance matrix (σ_{ij}):

$$P(r, z, t) = \frac{1}{2\pi\sigma_r(t)\sigma_z(t)\sqrt{1 - \rho_c^2(t)}}$$

$$\times \exp\left\{-\frac{1}{2(1-\rho_c^2(t))}\left[\frac{(r-\eta_r(t))^2}{\sigma_r^2(t)} - 2\rho_c(t)\frac{(r-\eta_r(t))}{\sigma_r(t)}\frac{(z-\eta_z(t))}{\sigma_z(t)} + \frac{(z-\eta_z(t))^2}{\sigma_z^2(t)}\right]\right\}, \quad (2)$$

where the correlation coefficient (ρ_c) is defined as

$$\rho_c(t) = \frac{\sigma_{rz}(t)}{\sigma_r(t)\sigma_z(t)}. \quad (3)$$

The ensemble mean particle locations needed in (2) can be obtained by numerical solution of the corresponding particle equations of motion. The simplified particle momentum equation, which neglects the Basset, virtual mass, Magnus, Saffman, and buoyancy forces can be written in terms of the particle relaxation time (τ_p) in cylindrical coordinates:

$$\frac{\mathrm{d}^2 z_p}{\mathrm{d}t^2} + \frac{1}{\tau_p}\frac{\mathrm{d}z_p}{\mathrm{d}t} = \frac{u_f}{\tau_p} + g, \quad (4a)$$

$$u_p = \frac{\mathrm{d}z_p}{\mathrm{d}t}, \quad (4b)$$

$$\frac{\mathrm{d}^2 r_p}{\mathrm{d}t^2} + \frac{1}{\tau_p}\frac{\mathrm{d}r_p}{\mathrm{d}t} - \dot{\theta}_p^2 r_p = \frac{v_f}{\tau_p}, \quad (4c)$$

$$v_p = \frac{\mathrm{d}r_p}{\mathrm{d}t}, \quad (4d)$$

$$\frac{\mathrm{d}w_p}{\mathrm{d}t} + \frac{1}{\tau_p}w_p = \frac{w_f}{\tau_p} - \dot{\theta}_p v_p, \quad (4e)$$

where the particle rate of rotation ($\dot{\theta}_p$) is expressed as

$$\dot{\theta}_p = \frac{w_p}{r_p}. \quad (4f)$$

The particle relaxation time (τ_p) in the above equations is defined in terms of particle and fluid physical properties, and the particle Reynolds number (Re_p) (Gosman and Ioannides [7]):

$$\tau_p = \frac{m_p}{3\pi d_p \mu_f}\frac{1}{(1+0.15\,Re_p^{0.687})}, \quad (5)$$

where

$$Re_p = \frac{\rho_f d_p |\vec{v}_d|}{\mu_f}, \quad (6)$$

and the particle drift velocity is given by

$$\vec{v}_d = \vec{u}_f - \vec{u}_p. \quad (7)$$

Equations (4)–(5) are valid for most practical flows where the turbulent intensities are lower than 20%, the particle-to-fluid density ratios are greater than 200, and the particle Reynolds number is less than 1000 (Clift et al. [35]; Shuen et al. [8]). These equations can be analytically solved over small time steps (Δt), over which the fluid velocity vector ($\vec{u}_f$) acting on the particle, the particle relaxation time, and the particle rotation rate are assumed constant.

Equations (4a)–(4e) solve for the instantaneous particle positions and velocities, but, in the present model the ensemble-averaged particle locations are needed in (2). Consequently, the equations (4a)–(4e) are solved for ensemble-averaged particle positions and velocities by evaluating the fluid and particle properties, such as $\vec{u}_f$, τ_p and $\dot{\theta}_p$, for the particle ensemble. In this model, these particle properties are estimated at the present time and held constant over the time step. For example, for the axisymmetric geometry, the fluid velocity vector acting on the particle ensemble is approximated from the knowledge of the particle PDF a given time by the following expression (Smith [36]):

$$\langle u_{f;i}\rangle(t) = \int_{-\infty}^{\infty}\int_{-\infty}^{\infty} \bar{u}_{f;i}(r,z)W(r,z,t)2\pi r\,\mathrm{d}r\,\mathrm{d}z, \tag{8}$$

where $\bar{u}_{f;i}$ is the Eulerian time-averaged fluid velocity and W is the weight function for the PDF. The Eulerian fluid velocity in (8) is available from the fluid phase solution. The expression for the weight function for the present geometry is (Baxter [37])

$$W(r,z,t) = \frac{P(r,z,t)}{\int_{-\infty}^{\infty}\int_{-\infty}^{\infty} P(r,z,t)2\pi r\,\mathrm{d}r\,\mathrm{d}z}. \tag{9}$$

In this model, the particle ensemble is tracked in the flow field until its ensemble mean location (η_z) leaves the computational domain. Furthermore, the interaction of the PDF with a boundary wall is approximated as simple reflection ([37]).

The central problem in this approach is to calculate the spatial spread of the ensemble (σ_{ij}) as it moves through the flow field. The basic equation for σ_{ij} is (Shirolkar and McQuay [4])

$$\sigma_{p;ij}(t) = \int_0^t\int_0^{t_2} \sqrt{\langle u'^2_{p;i}(t_2)\rangle}\sqrt{\langle u'^2_{p;j}(t_2)\rangle}\left[R^{\mathrm{L}}_{p;ij}(t_1,t_2) + R^{\mathrm{L}}_{p;ji}(t_1,t_2)\right]\mathrm{d}t_1\,\mathrm{d}t_2, \tag{10}$$

where the normalized Lagrangian particle correlation tensor ($R^{\mathrm{L}}_{p;ij}$) is defined as

$$R^{\mathrm{L}}_{p;ij}(t_1,t_2) = \frac{\langle u'_{p;i}(t_1)u'_{p;j}(t_2)\rangle}{\sqrt{\langle u'^2_{p;i}(t_2)\rangle}\sqrt{\langle u'^2_{p;j}(t_2)\rangle}}. \tag{11}$$

Shirolkar and McQuay [4] have shown that the Frenkiel functions (Frenkiel [38]) adequately model the tensor in (11). Thus

$$R^{\mathrm{L}}_{p;ij}(t_1,t_2) = \exp\left[\frac{-|t_1-t_2|}{(m^2+1)\tau_{p\,\mathrm{L}_{ij}}}\right]\cos\left[\frac{m|t_1-t_2|}{(m^2+1)\tau_{p\,\mathrm{L}_{ij}}}\right], \tag{12}$$

where m is a modeling parameter, referred to in the open literature as the negative-loop parameter (cf. [4]), and $\tau_{p\,\mathrm{L}_{ij}}$ is the particle Lagrangian time scale tensor.

The equation (10) can be numerically integrated, using (12), along the ensemble trajectory if the estimates for the particle Lagrangian time scale tensor ($\tau_{p\,\mathrm{L}_{ij}}$) and the particle fluctuating velocity variances at the present time ($\langle u'^2_{p;i}\rangle$) are known for the ensemble. The following sections show how these two particle properties are estimated for particle dispersion in axisymmetric swirling flows. Section 2.1.1 first discusses how the momentum source terms (S^{ϕ}_p) and particle Eulerian statistics are computed.

2.1.1. The particle Lagrangian time scales

Shirolkar and McQuay [4] have conducted detailed analysis regarding the Lagrangian particle time scales required in this approach. This section presents how their equations are adapted for the present problem.

The model of [4] states that

$$\tau_{p\,\mathrm{L}_{ij}} = \max(\tau_p, \tau_{sf\,\mathrm{L}_{ij}}), \tag{13}$$

where $\tau_{sf\,\mathrm{L}_{ij}}$ is the surrounding fluid time scale tensor. For isotropic turbulence, this tensor is expressed by the following equations ([4]):

$$\tau_{sf\,\mathrm{L}_{11}} = \tau_{sf\,\mathrm{L}_{22}} = \frac{TL_{f\,E_{33}}(\sqrt{L_{f\,\mathrm{E}_{33}}^2 + T^2 v_d^2} - 0.5Tv_d)}{L_{f\,\mathrm{E}_{33}}^2 + T^2 v_d^2}, \tag{14a}$$

and

$$\tau_{sf\,\mathrm{L}_{33}} = \frac{TL_{f\,\mathrm{E}_{33}}}{\sqrt{L_{f\,\mathrm{E}_{33}}^2 + T^2 v_d^2}}, \tag{14b}$$

where T is the fluid integral time scale seen by the heavy particle in the absence of drift velocity and $L_{f\,\mathrm{E}_{33}}$ is the fluid integral length scale of the longitudinal spatial velocity correlation of the Eulerian flow field. The expressions for T and $L_{f\,\mathrm{E}_{33}}$ are available in terms of a length scale ratio (β), the particle physical properties, and the turbulence characteristics of the flow (see [4]). All the fluid phase properties needed to compute T and $L_{f\,\mathrm{E}_{33}}$ are evaluated for the particle ensemble using expressions analogous to (8). It is important to note that the coordinate directions in (14) correspond to $i = 1$ and 2 for the transverse direction, and to $i = 3$ for the longitudinal direction; both are relative to the particle drift velocity.

In axisymmetric swirling flows, because of three forces (gravity, centrifugal and Coriollis) that simultaneously act on the particle at any instant of time, the particle drift direction continually changes from one region of the flow to another. Thus the equation (10) must be solved in a coordinate system that is rotated to align $i = 3$ with the particle drift velocity. *Figure 1* pictorially illustrates this rotation of the coordinate system, showing the particle's movement in discrete steps from A to B to C in the fixed $z-r$ coordinate system. The figure shows how the particle moves relative to the fluid particle that was initially located at the particle mean location. Due

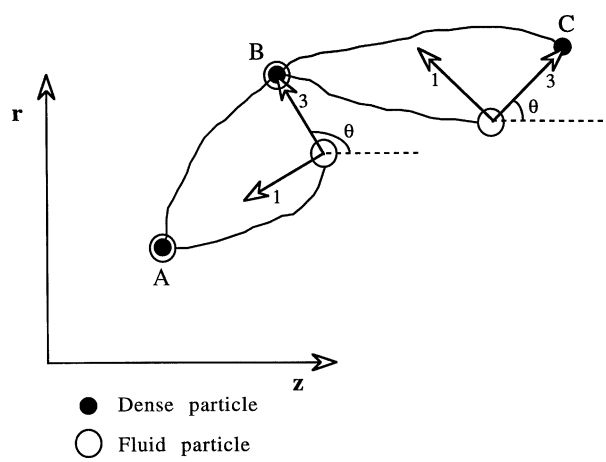

Figure 1. Transformation of coordinate system from $z-r$ to 3–1 as the dense particle moves in discrete steps.

to the two-dimensional nature of the present problem, the figure shows the two new coordinate directions ($i = 1$ and 3) in the $r-z$ plane.

At each time step, the drift velocity for the particle ensemble can be computed by using ensemble-averaged velocities in (7). This determines the direction of the particle's drift for that time step. All the relevant vectors and tensors needed to solve (10) for that time step are rotated in the new coordinate system by use of the following equations:

$$a_k^{\mathrm{N}} = a_j M_{jk}, \tag{15a}$$

$$A_{kq}^{\mathrm{N}} = A_{ji} M_{jk} M_{iq}, \tag{15b}$$

where the superscript N refers to the new coordinate system, and M is the transformation matrix. The expression for the transformation matrix is given in terms of the angle of rotation (refer to *figure 1*):

$$M = \begin{bmatrix} \cos\theta & -\sin\theta \\ \sin\theta & \cos\theta \end{bmatrix}. \tag{16}$$

After computing (10), all the vectors and tensors are rotated back to the original coordinate system by using the transformation matrix given in (16) with θ substituted by $-\theta$. This procedure is repeated at each time step until the ensemble mean particle location leaves the computational domain.

2.1.2. The particle variances calculation

The equation for the ensemble-averaged, particle-fluctuating velocity, covariance tensor is given by Shirolkar ([39]):

$$\frac{\mathrm{d}}{\mathrm{d}t}\langle u'_{p;i} u'_{p;j}\rangle + \frac{2}{\tau_p}\langle u'_{p;i} u'_{p;j}\rangle = \frac{1}{\tau_p}\big(\langle u'_{f;i} u'_{p;j}\rangle + \langle u'_{f;j} u'_{p;i}\rangle\big). \tag{17}$$

This equation assumes that the centrifugal and the Coriollis forces primarily influence the particle's mean motion, and their contributions in (17) can therefore be neglected. Equation (17) can be easily solved along the ensemble trajectory, provided that the fluid-particle correlation terms ($\langle u'_{f;i} u'_{p;j}\rangle$) are known at each time step.

The differential equation for $\langle u'_{f;i} u'_{p;j}\rangle$ can be derived in terms of the particle relaxation time, the surrounding fluid time scale, and the ensemble-averaged, fluid-fluctuating velocity, covariance tensor (Shirolkar [39]):

$$\frac{\mathrm{d}\langle u'_{f;i} u'_{p;j}\rangle}{\mathrm{d}t} + \left(\frac{1}{\tau_p} + \frac{1}{\underbrace{\tau_{sf\,\mathrm{L}_{ii}}}_{\substack{\text{No summation}\\ \text{intended here}}}}\right)\langle u'_{f;i} u'_{p;j}\rangle = \frac{1}{\tau_p}\langle u'_{f;i} u'_{f;j}\rangle. \tag{18}$$

The fluid tensor on the right-hand side of (18) can be obtained for the particle ensemble from the time-averaged fluid phase solution by using the weight function as shown in (8). Note that because of the turbulence isotropy assumption in this model, the time-averaged fluid tensor takes the form

$$\overline{u'_{f;i} u'_{f;j}} = \begin{cases} \frac{2}{3}k; & \text{for } i = j, \\ 0; & \text{for } i \neq j, \end{cases} \tag{19}$$

where k is the turbulent kinetic energy (refer to *table I*).

Equation (18) is solved in the new coordinate system (refer to *figure 1*), followed by (17). The variances required in (10) can be obtained by solving for the case $i = j$ in (17). However, due to the constant rotation of

the coordinate system and the nonisotropic nature of the tensor in (17), it is also necessary to solve (17) for the case $i \neq j$.

2.1.3. Calculations of the momentum source terms

The unique feature of the present model is that for each time step, momentum source terms are calculated for each and every Eulerian computational cell. This is achieved by distributing the particle momentum source for each time step according to the instantaneous spatial distribution of the particles. Mathematically, this translates into

$$S_p^{\phi}(i,j) = \sum_k \sum_t \dot{m}_{p;k} \Delta u_t^{\phi} \int_{\Delta z_i} \int_{\Delta r_j} W(r_j, z_i, t) 2\pi r \, \mathrm{d}r \, \mathrm{d}z, \tag{20}$$

where $\dot{m}_{p;k}$ is the particle mass flow rate for the kth particle ensemble; Δu_t^{ϕ} is the velocity change during tth time step; i and j refer to a particular Eulerian computational cell with the dimensions Δz_i and Δr_j.

In the SSF models, the momentum sources at each time step are added to the Eulerian cells along the particle trajectory. Therefore, such models rely on computing a large number of particle trajectories to adequately represent the particle phase. However, in the present model it is sufficient to track a few particle ensembles to properly distribute the sources.

2.1.4. Eulerian particle velocity statistics – The Markov-chain model

The PDFP model in its original form is not suited to compute the particle Eulerian statistics, such as time-averaged velocity and root-mean-square (rms) fluctuating velocity, which are available from the experiments. This study develops a method of generating the particle statistics that are required for comparison with the experimental data. This procedure of generating statistics is based on the exact same concepts as the original model; thus, it is possible not only to validate the basic principles of the PDFP approach, but also the procedures developed in this study to estimate various parameters, such as the particle Lagrangian time scales and the particle velocity variances.

A procedure to calculate individual particle trajectories is to solve for time-averaged particle velocities and mean particle locations by using time-averaged fluid phase velocities in equations (4). The instantaneous particle velocity vector and the particle position vector can be then obtained using the Markov-chain model that follows:

$$u_{p;i}(t) = \bar{u}_{p;i}(t) + u'_{p;i}(t), \tag{21a}$$

$$u'_{p;i}(t) = R^{\mathrm{L}}_{p;ii}(\Delta t) u'_{p;i}(t - \Delta t) + d_{t_i}, \tag{21b}$$

$$\overline{d_{t_i}^2} = \overline{u'^2_{p;i}} \left(1 - \left(R^{\mathrm{L}}_{p;ii}(\Delta t)\right)^2\right), \tag{21c}$$

$$x_{p;i}(t) = x_{p;i}(t - \Delta t) + \left(u_{p;i}(t) + u_{p;i}(t - \Delta t)\right) \frac{\Delta t}{2}, \tag{21d}$$

where d_{t_i} is a zero mean normal random vector independent of $u'_{p;i}(t - \Delta t)$. The variance of d_{t_i} is given in (21c). It should be noted that (21b) and (21c) are valid in the principal axis coordinate reference frame of the tensor $R^{\mathrm{L}}_{p;ij}$, and no summation is intended for the 'i' indexes in (21b) and (21c).

The principal axis coordinate frame for $R^{\mathrm{L}}_{p;ij}$ is the previously discussed reference frame, which is rotated to align axis '3' with the particle drift velocity (see *figure 1*). The particle drift direction can be established by using time-averaged velocities in (7). Once this is achieved, the time-averaged, particle-fluctuating velocity variance needed in (21c) can be obtained from the solution of the time-averaged equivalent of equations (17) and (18). These equations are also solved in the new reference frame. Thus, it is possible to solve for instantaneous

particle velocities (21a) and positions (21d) at discrete time steps. It is interesting to observe that unlike other stochastic models, this approach accounts directly for the time correlations in the particle-fluctuating velocities (21b).

In the present method, a large number of particle trajectories are tracked in the completely converged fluid flow field to calculate the Eulerian velocity statistics needed for comparisons with the experimental data. The above Markov-chain model is known to reproduce the solution of (10) when the dispersing particles are fluid elements. For example, several investigators have shown the equivalence between the Markov-chain model and the solution of (10), when studied for a simple case of point-source (fluid) particle dispersion in a stationary, homogeneous flow (Hanna [40]; Lamb et al. [41]; Reid [42]; Burry and Bergeles [12]; Shirolkar et al. [15]). Comparing the statistics obtained using this method with experiments is an indirect but valid procedure to evaluate the original PDFP approach.

2.2. The Lagrangian dispersion model based on eddy lifetime concept

The SSF model used in this study is conceptually similar to other eddy lifetime models applied to axisymmetric swirling flows (Azevedo and Pereira [43]; Sommerfeld et al. [44]). In this SSF model, the eddy lifetime and the eddy size needed to estimate the eddy-particle interaction time is obtained for the local turbulence properties as follows:

$$\tau_{f\,\mathrm{L}} = 0.3\frac{k}{\varepsilon}, \tag{22a}$$

$$l_e = \left(\frac{2}{3}k\right)^{0.5}\tau_{f\,\mathrm{L}}, \tag{22b}$$

where the constant '0.3' in (22a) is based on the computer optimization study of Milojevic [1], who used the experimental data of Snyder and Lumley [5] to determine its value.

The eddy lifetime model implemented here is not limited to sampling the fluctuating fluid-velocity vector that acts on the particle during a particular time step from equation (19), which assumes turbulence isotropy. This model has the option of sampling these fluctuating velocities from the estimates for Reynolds stresses ($\overline{u'_{f;i}u'_{f;j}}$). These estimates are based on a set of second-order algebraic relations (Rodi [45]):

$$\overline{u'_{f;i}u'_{f;j}} = \frac{2}{3}k\delta_{ij} + \frac{k}{\Phi/\bar{\rho} - \varepsilon + C'_1\varepsilon} \times \left[(1-\gamma_1)\left(P_{ij} - \frac{2}{3}\delta_{ij}\Phi/\bar{\rho}\right) - \gamma_2 k\left(\frac{\partial \bar{u}_{f;i}}{\partial x_j} + \frac{\partial \bar{u}_{f;j}}{\partial x_i}\right) - \gamma_3\left(D_{ij} - \frac{2}{3}\delta_{ij}\Phi/\bar{\rho}\right)\right], \tag{23a}$$

where

$$P_{ij} = -\left(\overline{u'_{f;j}u'_{f;k}}\frac{\partial \bar{u}_{f;i}}{\partial x_k} + \overline{u'_{f;i}u'_{f;k}}\frac{\partial \bar{u}_{f;j}}{\partial x_k}\right) \tag{23b}$$

and

$$D_{ij} = -\left(\overline{u'_{f;j}u'_{f;k}}\frac{\partial \bar{u}_{f;k}}{\partial x_i} + \overline{u'_{f;i}u'_{f;k}}\frac{\partial \bar{u}_{f;k}}{\partial x_j}\right). \tag{23c}$$

The above model constants C'_1, γ_1, γ_2, and γ_3 are set at 1.8, 0.76, 0.18, and 0.11, respectively (Picart et al. [46]). These relations are derived for axisymmetric swirling flows (Shirolkar [39]). They are solved prior to the particle calculations, using a predictor-corrector algorithm recommended by Picart et al. [46].

The particle-wall collisions are modeled as simple reflections. It is assumed that the particles do not lose any momentum in the velocities parallel to the wall. However, a coefficient of restitution (0.9) is applied in the reflected velocity normal to the wall (Azevedo and Pereira [43]). This particle-wall collision model is also employed in the Markov-chain model. Other details on the eddy lifetime model used here can be found in Coimbra et al. [47].

3. Results from the model validation study

The experiments of Sommerfeld and Qiu [29] involved the measurement of particle statistics in a cylindrical reactor. The rector configuration is shown in *figure 2*, which illustrates a central, particle-laden, primary jet and a coaxial, swirling, secondary jet entering the test section. The figure also shows the coordinate directions z and r. The reactor is modeled assuming axisymmetry. The dimensions of the reactor and the inlet flow conditions are summarized in *table II*.

In the simulations, experimental profiles available at $z = 3$ mm were used as inlet conditions. The gas phase equations were solved on a 100×75 grid. The zero-gradient outlet boundary condition was set at $z = 1.0$ m (Sommerfeld et al. [44]). The inlet kinetic energy and the dissipation rate for the k–ε model were specified as (Sommerfeld and Wennerberg [48])

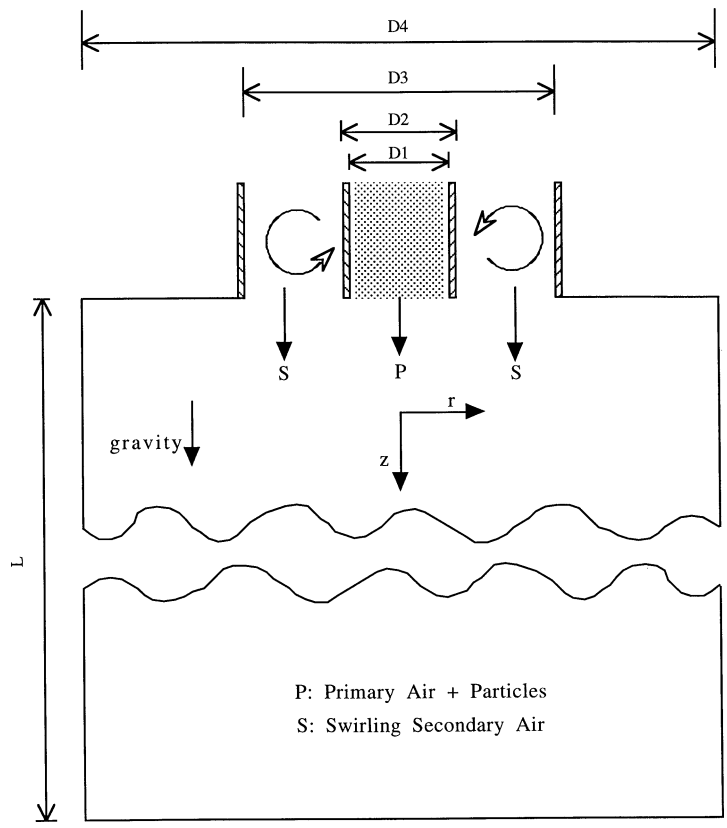

Figure 2. Illustration of the experimental setup used by Sommerfeld and Qiu [29].

Table II. Geometric and inlet conditions for the experiments of Sommerfeld and Qiu.

Geometric Parameters (refer *figure 2*)	
$D1$ (mm)	32
$D2$ (mm)	38
$D3$ (mm)	64
$D4$ (mm)	194
L (m)	1.5
Inlet Conditions	
Primary Air Flow Rate (g/s)	9.9
Secondary Air Flow Rate (g/s)	38.3
Inlet Reynolds Number (based on $D3$)	52400
Swirl Number	0.47
Particle Mass Flow Rate (g/s)	0.34
Particle Loading	0.034

$$k = \frac{1}{2}\left(u'^2_{f_{\text{inlet}}} + v'^2_{f_{\text{inlet}}} + w'^2_{f_{\text{inlet}}}\right), \tag{24a}$$

$$\varepsilon = \frac{c_\mu k^{3/2}}{0.03D}, \tag{24b}$$

where D is the characteristic dimension of the inlet flow passage. For the MTS model, a highly non-equilibrium condition was used to estimate the inlet turbulence quantities (Chen [49]):

$$k_p = k_t = 0.5k, \tag{25a}$$

$$\varepsilon_p = 0.5\varepsilon_t = 0.5\varepsilon, \tag{25b}$$

where k and ε are given in (24). This study found that using (25) as an inlet condition for the turbulence quantities in the MTS model gave the best results compared with other possible conditions, such as $k_p/k_t = 4.0$ and $\varepsilon_p/\varepsilon_t = 1.0$.

The particles used in the experiments were solid glass beads ($\rho_p = 2500$ kg/m^3). The inlet particle size distribution approximated the following log-normal distribution (Sommerfeld and Wennerberg [48]):

$$f(d_p) = \frac{1}{\sqrt{2\pi}\sigma d_p} \exp\left(\frac{-(\ln d_p - \ln d_m)^2}{2\sigma^2}\right), \tag{26}$$

where $\sigma^2 = 0.18$ and $d_m = 44.3$ μm. The above size distribution was used to determine the percentage of particles present in 10 equal size bins. Thus, for the purpose of modeling, the particle phase was represented by 10 different monosized particles with the appropriate mass fractions.

In the PDFP model, each particle calculation involved computing 10 particle ensembles (corresponding to the ten particle sizes) with a specified initial mean location and initial variance. Because experimental data showed that the inlet particle distribution was fairly even across the primary tube, the initial mean and the lateral variance were determined from a uniform distribution function (Papoulis [50]). At the inlet location, the fluid phase properties needed for the particle ensemble were weighted by using this uniform distribution function.

The loop parameter in (12) and the length scale ratio needed to estimate the time and length scales in (14) were based on the findings of Shirolkar and McQuay [4]. The particles used in the experiments had a mean Stokesian response time of 15.6 msec and were subjected to external forces, such as gravity. Therefore, the loop

parameter was set equal to 1, as the particles were expected to be influenced by the crossing trajectories effects (CTE). The length-scale ratio (β) was set equal to 0.39; this value gave the best predictions when compared with the experiments of Snyder and Lumley [5] (refer to results from Shirolkar and McQuay [4]). This choice of β is also consistent with the constant used to determine the fluid Lagrangian time scale in several time-correlated dispersion models (Berlemont et al. [11]; Burry and Bergeles [12]; Lu et al. [13]; Chen and Pereira [14]).

Burry and Bergeles [12] have studied the influence of time step (Δt) on the predicted dispersion in homogeneous turbulence. They have showed that using time steps as high as 10 times the corresponding Lagrangian time scale can correctly account the turbulent dispersion. However, due to the complex nature of the present flow, the particle ensemble was restricted to cross only one local Eulerian computational cell at each time step. It was observed that, with such restriction, the time step in the PDFP model was always less than twice the particle Lagrangian time scale ($\tau_{p\,\mathrm{L}_{11}}$). As expected, the predictions were practically unaffected ($<1\%$) by using time steps as low as 0.1 times the particle Lagrangian time scale.

In the PDFP model it was observed that because of the constant rotation of the coordinate system, the correlation coefficient (ρ_c) in (3) acquired finite but negligible values ($\sim 10^{-2}$). Therefore, the coefficient was neglected for the purpose of calculating the weight function.

In the SSF model, the inlet mass flux measurements available at five distinct radial locations were used to determine the required number of initial particle trajectories starting from the primary tube. It was observed that a minimum of 340 particle trajectories originating from five distinct starting locations were required to achieve conformity with the measured inlet mass flux. Thus, for the SSF model, considering 10 discrete particle sizes, each particle calculation involved a total of 3400 trajectories. Similar to other models, the time step in the SSF model was set equal to the minimum of (i) the time required to cross one local Eulerian cell, and (ii) the eddy-particle interaction time.

3.1. Results from the preliminary studies

Preliminary studies were performed using the k–ε model for the gas phase, coupled with the two different models for the particle phase. The primary objectives were (i) to compare the computational efficiency of the two dispersion models, and (ii) to design an effective procedure that would validate the models used in this study, with particular emphasis on the PDFP approach. These two issues are discussed below.

Figures 3(a) and *3(b)* depict the gas velocity vectors and particle trajectories predictions for the present case. *Figure 3(a)* shows the ensemble mean particle trajectories predicted by the PDFP model. As explained earlier, this model also predicts the spatial spread (variances) along these mean trajectories. Thus, a small number of particle ensembles are sufficient to properly distribute the particle momentum source terms to the gas phase. In contrast to the PDFP model, the SSF model relies on computing a large number of particle trajectories in order to adequately represent the particle phase. This can be seen in *figure 3(b)*, which shows a typical SSF model trajectory prediction of 100 particle trajectories.

Figure 3 shows that the main characteristics of a swirling flow are the central recirculation zone (CRZ) and the external recirculation zone (ERZ). In this study it was observed that the presence of particles influences the predicted end points of the CRZ. For example, the k–ε model predicts that without the influence of particles, the CRZ extends from 77 mm to 284 mm. Whereas, by accounting for the presence of particles using the PDFP approach, the CRZ extends from 84 mm to 288 mm. The k–ε model when used in conjunction with the SSF particle model, predicted the end points to be 83 mm and 285 mm. It thus appears that the presence of particles has some measurable effect on the upstream gas phase predictions despite low particle loading (refer to *table II*).

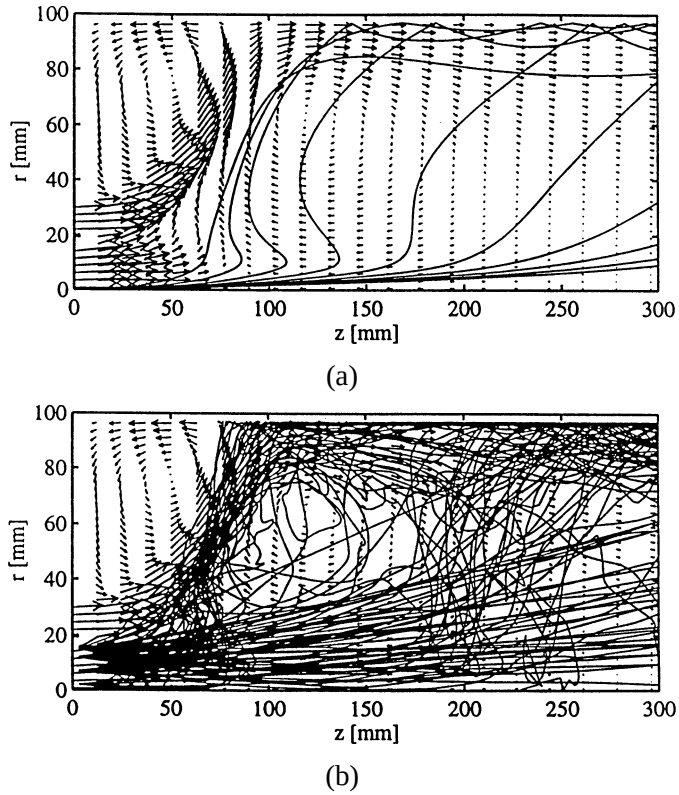

Figure 3. Predicted particle trajectories and gas velocity vectors in a swirling flow: (a) the particle ensemble trajectories obtained from the PDFP model coupled with the $k-\varepsilon$ model for gas phase, and (b) the individual particle trajectories obtained from the SSF model coupled with the $k-\varepsilon$ model for gas phase.

In this study it was found that 3400 particle trajectories per particle calculation and a total of 3 particle calculations were sufficient in the SSF model. Any further increase on the number of particle trajectory calculations had virtually no effect on the gas phase predictions. The total number of particle trajectories in this case were very small considering that the number of trajectories per particle size per starting location required to properly account for particle dispersion using a SSF model ranges from 2000 to 5000 (Baxter [37]). According to these estimates, for 10 discrete sizes and 5 distinct starting locations, a minimum of 100 000 particle trajectories would be needed to properly account for particle dispersion. The small number of particle trajectory calculations required in this case to measure the influence of particles on the gas phase predictions is due mainly to the very low particle loading.

The PDFP model also required a total of 3 particle calculations (a total of 30 ensembles). As in the case of the SSF model, any further increase in the number of particle calculations in the PDFP model had an insignificant effect on the gas phase predictions. The total CPU time on a HP UNIX workstation (715/64 SPU) for the PDFP model per particle calculation (i.e., 10 ensembles) was 0.83 min. Whereas, the SSF model required about 2.14 min per particle calculation (i.e., 3400 trajectories). Thus, even in the case of very low particle loading, the PDFP approach reduces the particle computational time by more than half compared to the SSF model. The computational advantage of the PDFP model is expected to be very significant in situations where the particles have a greater impact on the carrier phase.

The computational burden in the PDFP approach is concentrated in calculating the weight function in (9). Theoretically, the assumed Gaussian shape for the particle ensemble is appropriate (Litchford and Jeng [51]).

However, computationally it is costly compared to other shapes, such as the uniform or the isosceles triangle PDF's. Litchford and Jeng [51] studied their statistical dispersion model sensitivity to the shape of the particle positional PDF. Their results indicate that, in comparison to the Gaussian PDF, the isosceles triangle PDF provides improved computational efficiency without sacrificing numerical accuracy. This result was later confirmed by Chen and Pereira [20] while studying numerical predictions for a confined evaporating spray. Such practical approximations would also further benefit the computational efficiency of the PDFP approach.

The above discussion indicates the indubitable potential of the PDFP approach in efficiently distributing the particle source terms. However, it must still be determined whether or not the present method can correctly account for the dispersion phenomenon. This can be achieved by comparing the model predictions with the experimental data. The PDFP model can predict Lagrangian particle statistics, and these predictions can be compared directly with experiments that also measure Lagrangian statistics (for example, experiments of Snyder and Lumley [5], and Wells and Stock [6]). However, the particle statistics available from the experiments of Sommerfeld and Qiu [29] are the mean and the rms fluctuating velocity radial profiles at several different axial locations inside the reactor. Consequently, it is not possible to compare the PDFP model predictions directly with these Eulerian particle statistics, and the present study thus takes a two-step approach to validate the PDFP model: (i) evaluate the gas phase results obtained by using the PDFP model to account for the presence of particles; and (ii) evaluate the Eulerian particle velocity statistics predicted by the Markov-chain model. It should be noted that as previously discussed, the Markov-chain model is equivalent to the PDFP approach. This study also compares the SSF model predictions with the Markov-chain model predictions and the experimental data.

The results from this model-validation study are presented in three sections. In the first part, the gas phase results that were obtained by using the two different turbulence models and the two dispersion models are discussed. The discussion focuses mainly on the predictions obtained using the two turbulence models coupled with the PDFP model for the particle phase. The predicted gas phase results are evaluated with the experimental data. In the second part, the particle mean velocities predicted using the Markov-chain model are compared with the experiments. In this section the particle statistics are calculated in two different gas flow fields – the k–ε and the MTS model predictions coupled with the PDFP model for the particle phase. In the third section, the particle velocity statistics (mean and rms fluctuating velocities) that were obtained by using both the Markov-chain model and the SSF model are compared with the experimental data. The gas phase results used to generate these statistics are the same as those obtained by using the MTS model coupled with the respective particle models.

The predicted radial profiles for gas and particle velocities (both mean and rms fluctuating velocities) are compared with the experimental data at several axial locations. The figures presented below typically show predictions at $z = 3$ (which is used as the inlet condition for the models), 52, 112, 155, 195, and 315 mm. Note that, the locations $z = 112$, 155, and 195 mm are located inside the CRZ. The experiments of Sommerfeld and Qiu [29] were previously simulated at the fifth workshop on two-phase flow predictions (refer to case 3 in Sommerfeld and Wennerberg [48]). The discussion that follows makes references to the predictions presented at this workshop, in particular to the predictions of Azevedo and Pereira [43], and Ando and Sommerfeld [52]. The workshop simulation results were presented for the axial stations of $z = 52$, 155, 195, and 315 mm. Sommerfeld et al. [44] have also simulated these experiments and presented their particle phase predictions at $z = 52$, 112, 195, and 315 mm.

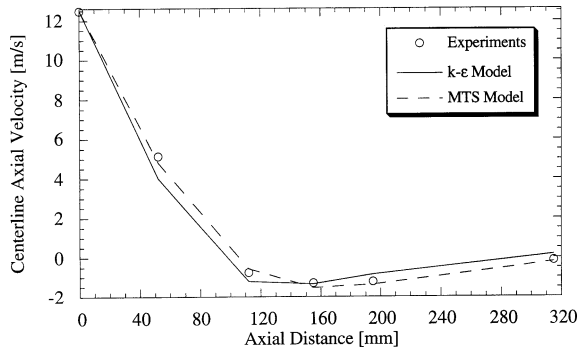

Figure 4. Comparison between the experiments and the predicted centerline gas axial mean velocity. Experiment: ○. Simulation: ——, $k-\varepsilon$ model with PDFP model; – – –, MTS model with PDFP model.

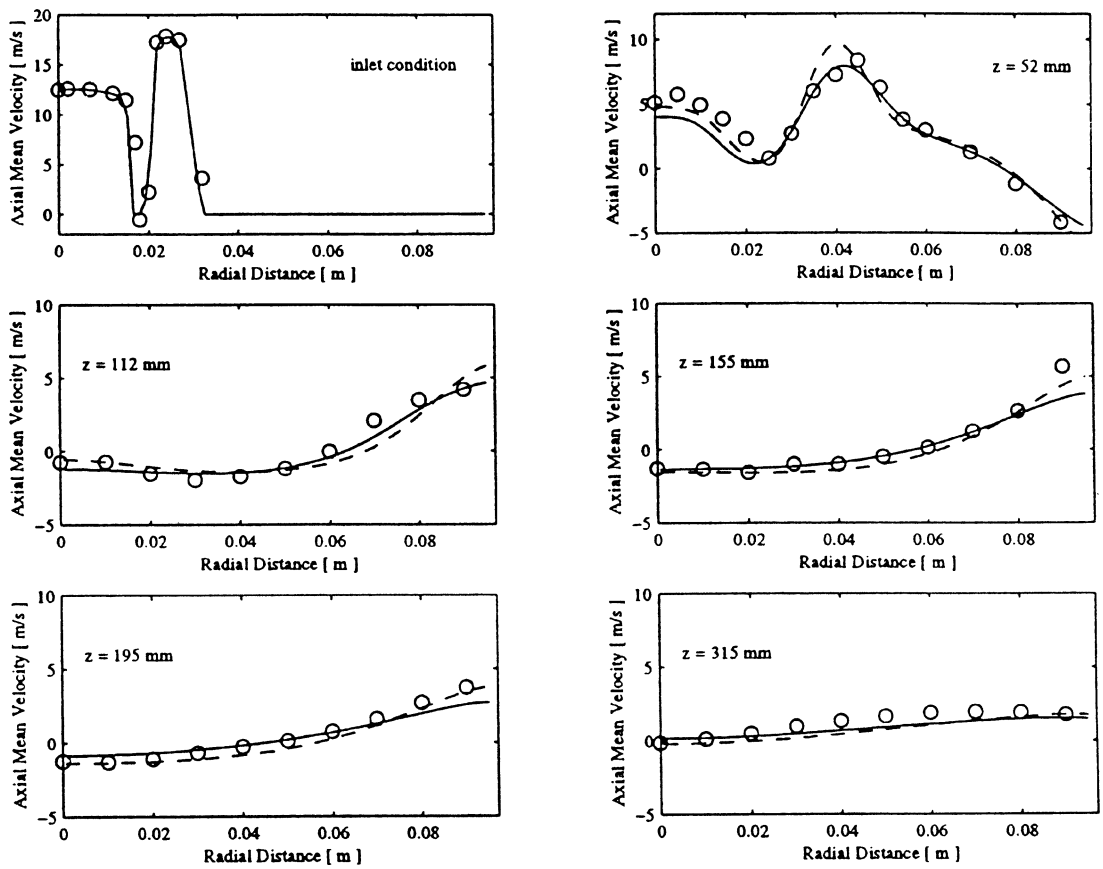

Figure 5. Comparison between the experiments and the predicted gas axial mean velocity at different axial locations. Experiment: ○. Simulation: ——, $k-\varepsilon$ model with PDFP model; – – –, MTS model with PDFP model.

3.2. Fluid phase results

The fluid phase equations were solved using the two different turbulence models, and in both cases the PDFP model was used to account for the presence of the particle phase. As indicated before, the region of interest in swirling flows is the CRZ. The k–ε model predicted the CRZ to extend from 84 mm to 288 mm, while the MTS

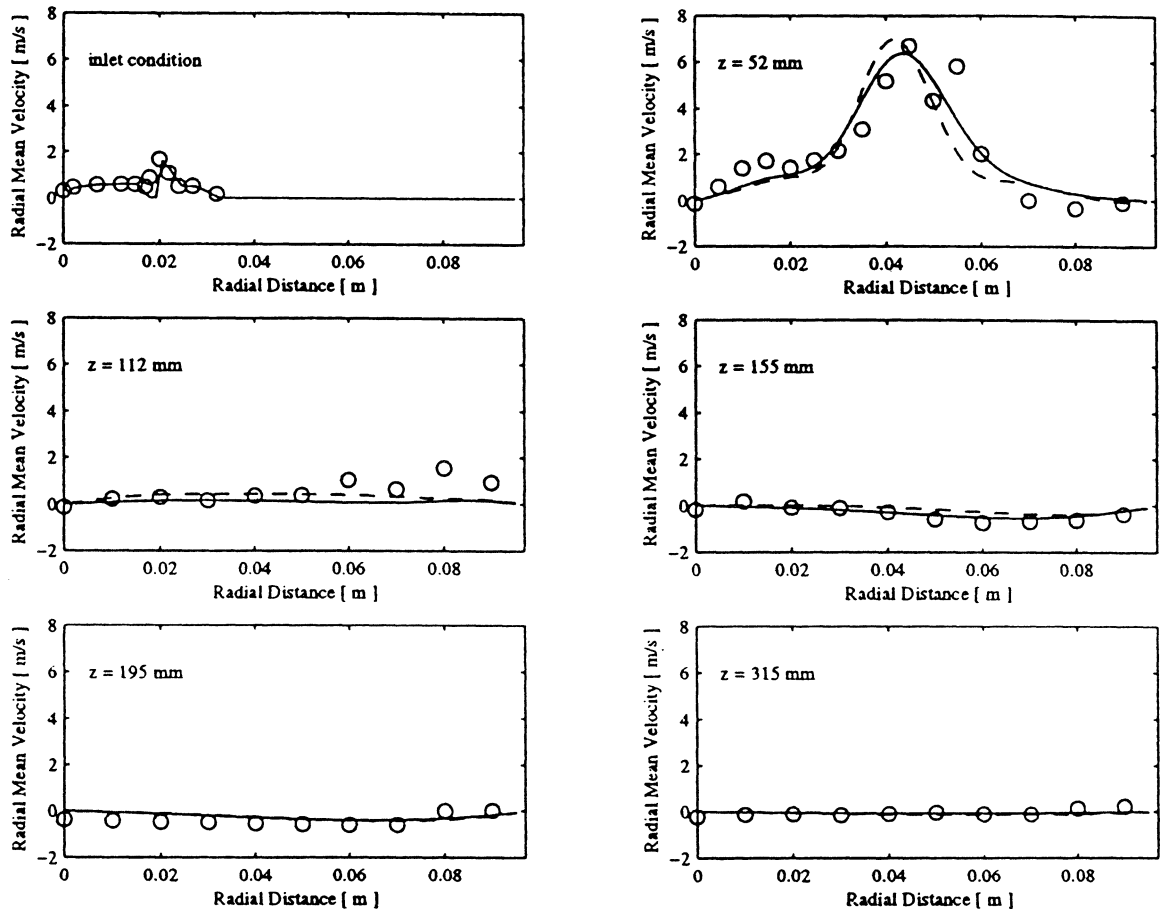

Figure 6. Comparison between the experiments and the predicted gas radial mean velocity at different axial locations. Experiment: ○. Simulation: ——, $k-\varepsilon$ model with PDFP model; – – –, MTS model with PDFP model.

model predicted it to be from 104 mm to 350 mm. Experimental data indicate that the CRZ extended from approximately 100 mm to 330 mm (see *figure 3* in Sommerfeld et al. [4]). Thus, it appears that the MTS model does a better job at predicting the CRZ. In order to confirm this observation, the gas centerline axial predicted mean velocity is compared with the experimental data in *figure 4*. The figure shows predictions from both the turbulence models. It is obvious from the figure that the MTS model predictions are better compared to the k–ε model.

Figure 5 compares the gas axial mean velocity predictions at several different axial locations with the experimental data. The solid lines in this figure show the k–ε model predictions, and the dashed lines represent the MTS model predictions. The figure shows that both models compare reasonably to the predictions; however, in regions close to the centerline and near the wall, the MTS model appears to predict the velocities more accurately than the k–ε model.

Figure 6 compares the gas radial mean velocity predictions with the experiments. The figure shows that both models compare favorably with the experiments. The slight discrepancy between the predictions and the experimental data at the near-wall location for $z = 112$ mm can also be observed in Sommerfeld et al. [44]. The gas tangential mean velocity predictions are compared with the experimental data in *figure 7*. The figure

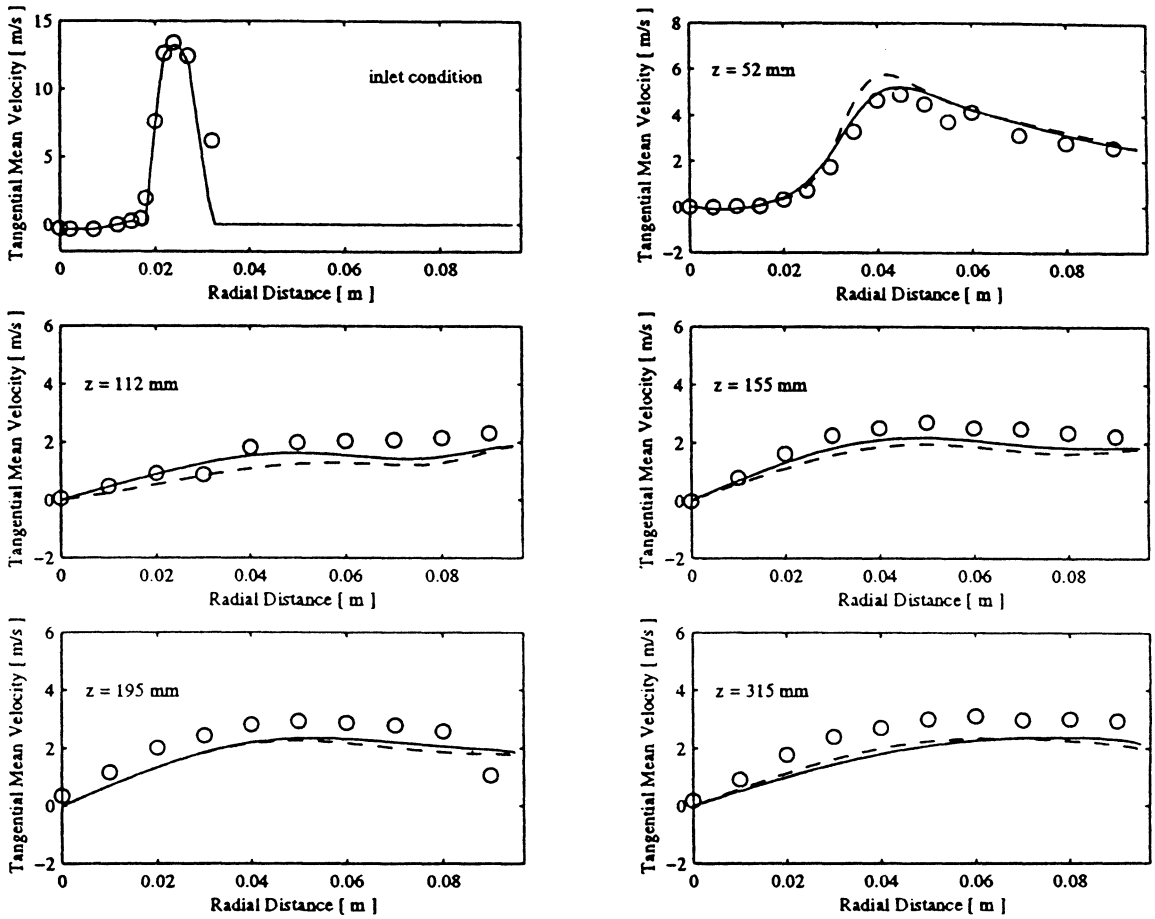

Figure 7. Comparison between the experiments and the predicted gas tangential mean velocity at different axial locations. Experiment: ○. Simulation: ——, k–ε model with PDFP model; – – –, MTS model with PDFP model.

shows that the models slightly underpredict the gas tangential velocity inside the CRZ. This discrepancy is also observed in [44].

In summary, the predicted gas mean velocities using both the turbulence models compared favorably to the experiments. The MTS model can more accurately predict the size of the CRZ, and is also superior to the k–ε model in predicting gas axial mean velocities near the centerline and the reactor wall.

Both the particle dispersion models used in this study rely on the gas rms fluctuating velocity predictions (refer to (19) and (23)), but the dependence of the SSF model on these predictions is more direct because it relies on these predictions to determine the instantaneous fluid velocity vector acting on the particle. Thus the predictions shown below are for turbulence models that use the SSF model for the particle phase. The algebraic relations used in this study are solved prior to the trajectory calculations in the SSF model.

Figure 8 compares the predictions obtained using the algebraic relations for the three components of the gas rms fluctuating velocity with the experimental data. The solid lines in the figure represent the predictions that were based on the k–ε model, and the dashed lines represent those that were based on the MTS model. The figure also shows the k–ε model predictions that assume gas phase isotropy (i.e., equation (19)). It is apparent from this figure that the models generally underpredict the rms fluctuating velocities, but, the algebraic relations

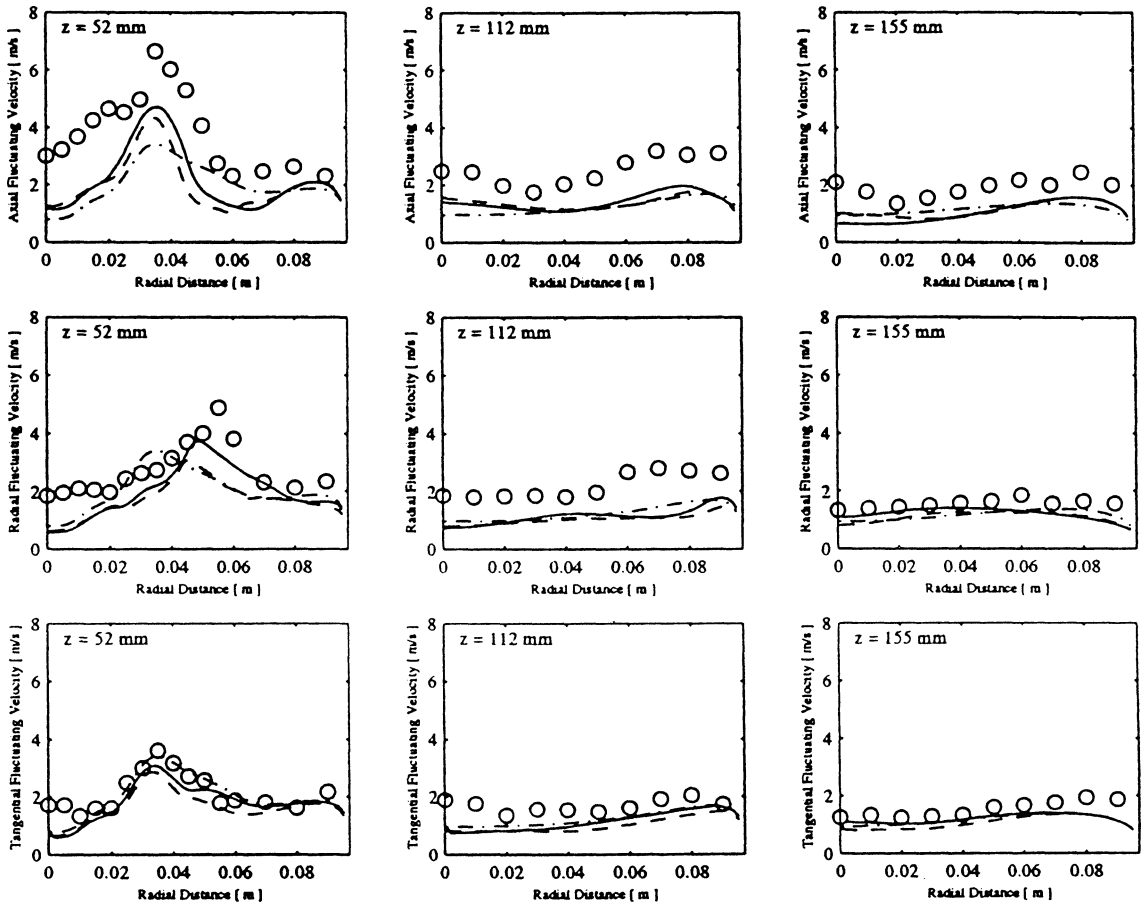

Figure 8. Comparison between the experiments and the predicted gas rms fluctuating velocities at three different axial locations. Experiment: ○. Simulation: ——, Algebraic relations ($k-\varepsilon$ model with SSF model); – – –, Algebraic relations (MTS model with SSF model); — - —, Turbulence isotropy assumption ($k-\varepsilon$ model with SSF model).

based on the k–ε model appear to give the best predictions. The underprediction of the gas fluctuating velocity has also been observed by several other investigators (refer to case 3 in Sommerfeld and Wennerberg [48]).

3.3. Evaluation of the Markov-chain model

The particle statistics presented in this section are calculated in two different gas flow fields. Predictions for both, the first gas flow field calculated using the k–ε model and the second using the MTS model, are shown in *figures 5–7*. The particle trajectories are generated in these flow fields by using the Markov-chain technique. More than 150 000 particles are tracked in the flow to calculate the particle average velocities, and the particle rms fluctuating velocities. The results for average velocities are presented in this section; the rms velocity results are presented in the next section.

The particle axial, radial, and tangential mean velocity predictions are compared with the corresponding experimental data in *figures 9*, *10*, and *11*, respectively. The solid lines in these figures indicate predictions obtained with the k–ε model for the gas phase, whereas, the dashed lines represent the predictions obtained with the MTS model for the gas phase. *Figure 9* shows that the model predictions for the particle axial velocity

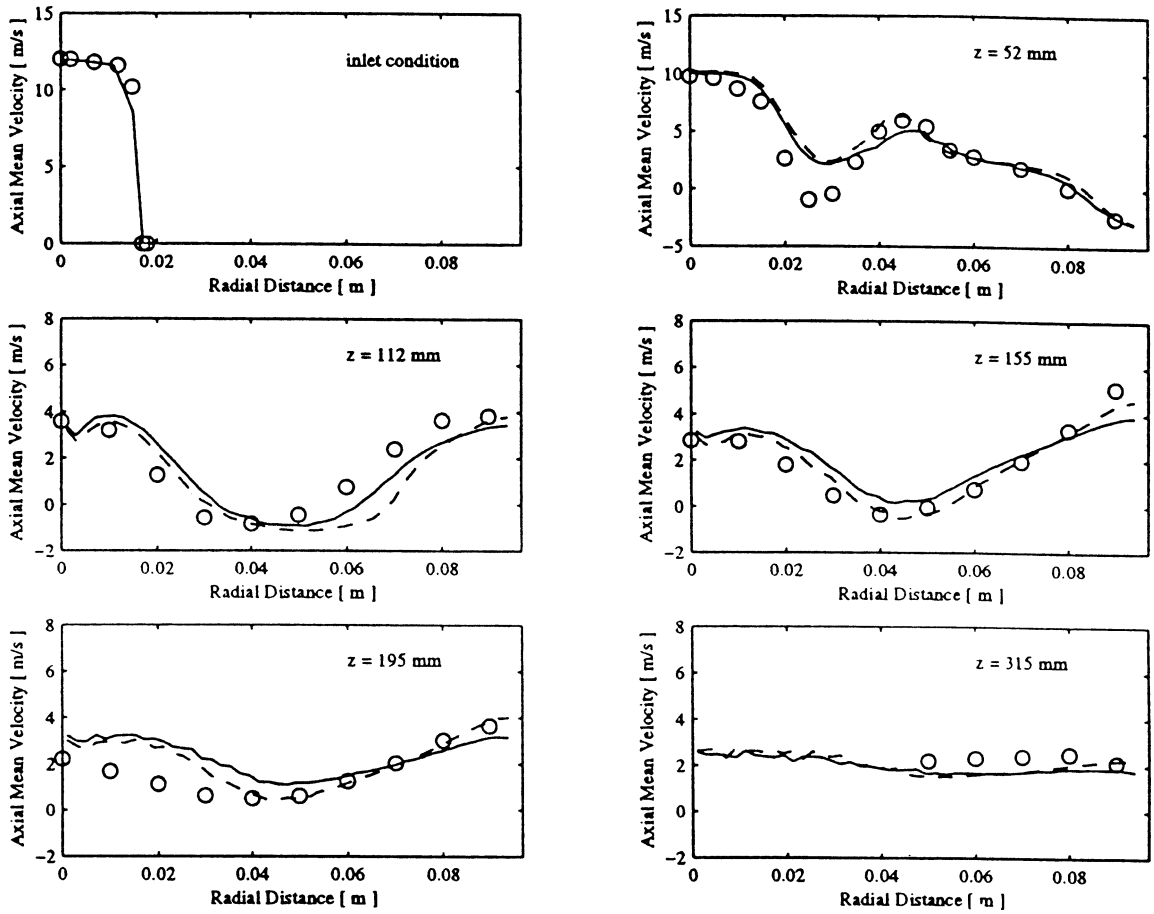

Figure 9. Comparison between the experiments and the Markov-chain model predictions, in two different gas fields, for the particle axial mean velocity at different axial locations. Experiment: ○. Simulation: ——, $k-\varepsilon$ model with PDFP model; – – –, MTS model with PDFP model.

compare very well with the experiments. The figure also indicates that, similar to the gas phase results, the particle predictions obtained with the MTS model for the gas phase are better compared to the k–ε model, especially in the near-wall region. The particle axial mean velocity predictions based on the k–ε model as shown in *figure 9*, are remarkably similar to the SSF model predictions of Sommerfeld et al. [44]. It should be noted that Sommerfeld et al. computed their particle statistics in a gas flow field obtained by using the k–ε model for turbulence.

The model comparisons shown for the present case during the 5th workshop on two-phase flow predictions were based almost exclusively on the k–ε model for gas phase (refer to case 3 in Sommerfeld and Wennerberg [48]). At that workshop, the SSF model of Azevedo and Pereira gave the best predictions for particle mean velocity in the region near the wall inside the CRZ. Their near-wall predictions were very close to the corresponding k–ε model predictions shown in *figure 9*. However, unlike the present predictions using the k–ε model for gas phase, the model of Azevedo and Pereira generally underpredicted the particle axial velocity inside the CRZ. The particle mean velocity predictions of Ando and Sommerfeld (also an SSF model), presented at the workshop, were quite similar to the present predictions that used the k–ε model for gas phase, except in the near-wall region. The model of Ando and Sommerfeld severely underpredicted (about 20% more than present simulations) the particle velocity in the region near the wall.

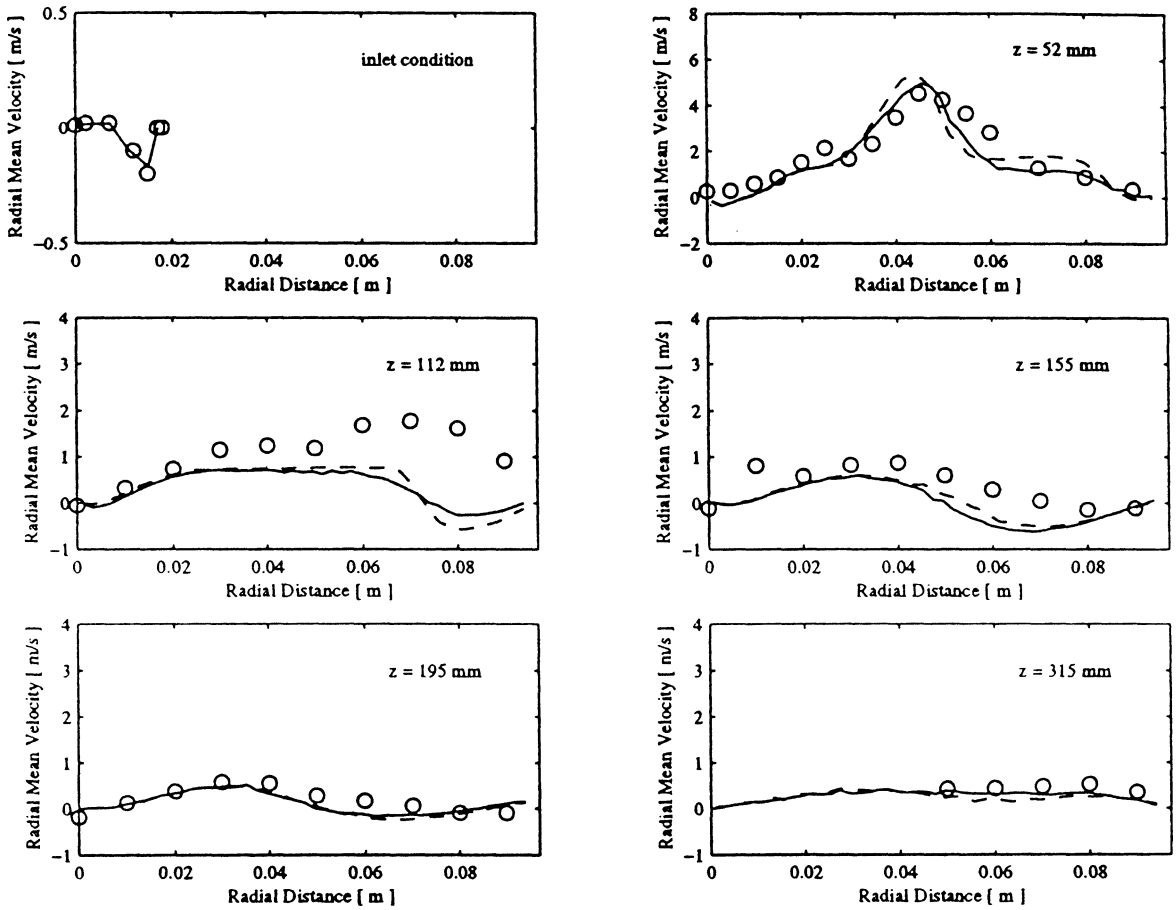

Figure 10. Comparison between the experiments and the Markov-chain model predictions, in two different gas fields, for the particle radial mean velocity at different axial locations. Experiment: ○. Simulation: ——, $k-\varepsilon$ model with PDFP model; – – –, MTS model with PDFP model.

Figure 10 shows that the model predictions compare satisfactorily with the experimental data for the particle mean radial velocity except at the axial location $z = 112$ mm. Like the gas phase results (*figure 6*), the velocity at this axial location in the near-wall region is also underpredicted by the particle model. This discrepancy is likewise reflected in the predictions of Sommerfeld et al. [44]. Note that, the results at this axial location were not reported in Sommerfeld and Wennerberg [48].

Figure 11 shows that the model underpredict the particle mean tangential velocities in the near-wall region inside the CRZ; this is a direct reflection of the discrepancy observed in the gas phase predictions (refer to the discussion on *figure 7*). Once again, these predictions are consistent with those of Sommerfeld et al. [44].

In summary, the particle mean velocity statistics based on the k–ε model for gas phase are consistent with the best predictions for this case in the current literature. The axial mean velocity predictions based on the MTS model for gas phase are an improvement over the corresponding k–ε model predictions, especially in the near-wall region inside the CRZ. The mean gas flow results have a direct effect on the particle mean velocity statistics. Discrepancies in the gas phase results are also reflected in the particle results. Finally, it appears that the predictions based on the concepts developed in this study to model the dispersion phenomenon are similar to those available from the stochastic models based on the eddy lifetime approach.

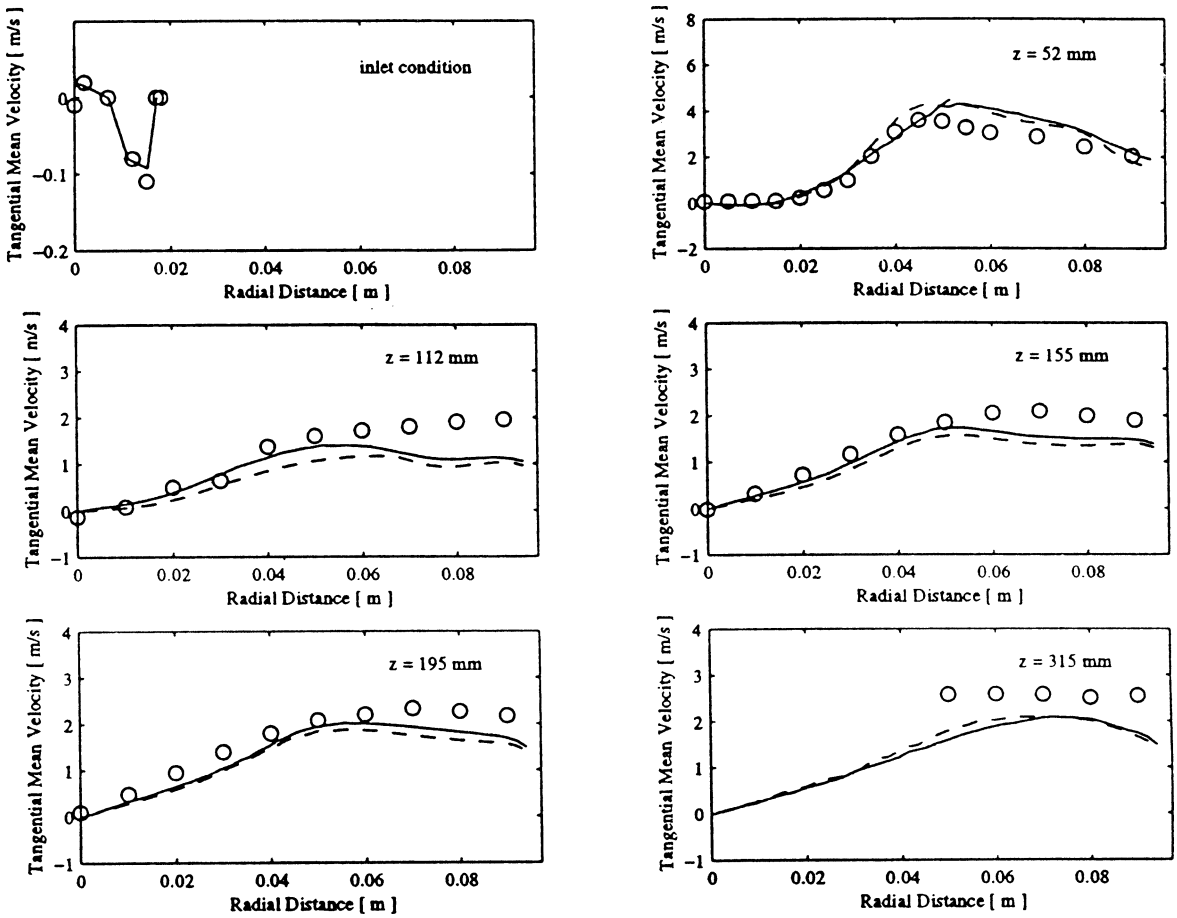

Figure 11. Comparison between the experiments and the Markov-chain model predictions, in two different gas fields, for the particle tangential mean velocity at different axial locations. Experiment: ○. Simulation: ——, $k-\varepsilon$ model with PDFP model; – – –, MTS model with PDFP model.

3.4. Direct comparison of the two approaches for dispersion modeling

The results presented in the previous section appear to indicate that the particle velocity statistics obtained by using the Markov-chain model are similar to those obtained from an SSF model. This section compares the predictions of these two models. The gas phase results used to compute the statistics were based on the MTS model for turbulence closure. In the SSF model, the gas fluctuating velocity vector is sampled from the solution of second-order algebraic relations (23).

The particle mean velocity predictions using the Markov-chain model and the SSF model are compared with the experimental data in *figure 12*. The figure shows the three velocity components at three different axial locations inside the reactor. The solid lines represents the predictions obtained by using the Markov-chain model; the dashed lines correspond to the SSF model predictions. The figure shows remarkable correspondence between the two models. Comparison with experiments for both models is also good.

The particle axial, and radial fluctuating velocity results at three different axial locations ($z = 52$, 115, and 195 mm) are shown in *figure 13*. The figure shows discrepancies between the predictions and the experiments. Despite these discrepancies, it appears that the predictions follow the trends observed in experiments involving the rms fluctuating velocity profiles. Inside the CRZ, both models overpredict the axial fluctuating velocity near

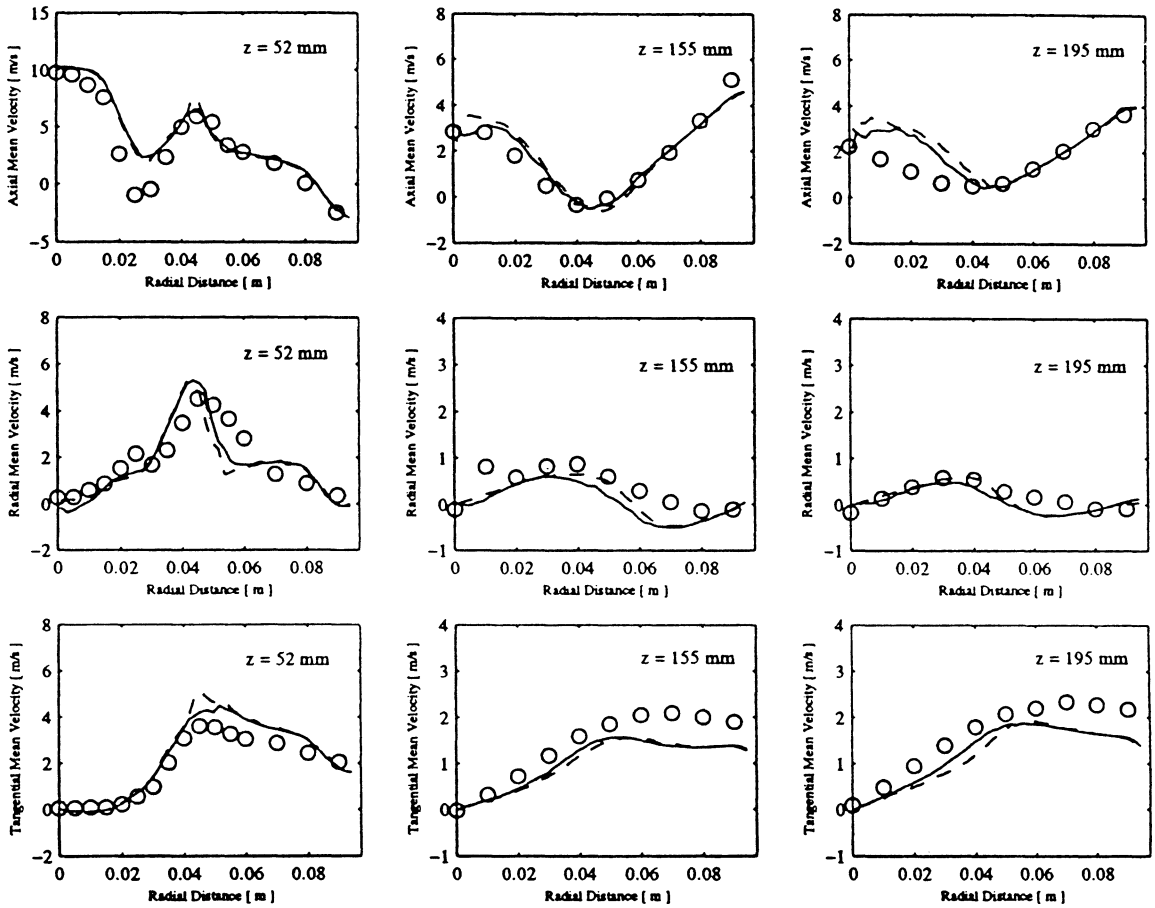

Figure 12. Direct comparison between the experiments and the predictions obtained using the Markov-chain model and the SSF model for the particle mean velocities at three different axial locations. Experiment: ○. Simulation: ——, Markov-chain model; – – –, SSF model.

the centerline, and underpredict it near the reactor wall. The particle rms radial fluctuating velocity results show that the models generally underpredict this component of the velocity. Sommerfeld et al. [44] also observe such discrepancies.

The particle rms fluctuating velocity results shown in *figure 13* seem to indicate that the differences observed in the predicted gas rms velocities (see *figure 8*) have little impact on these particle statistics. This is because the Markov-chain model is based on the turbulence isotropy assumption (19), while the SSF model uses algebraic relations to sample the gas fluctuating velocity (23). Shirolkar [39] confirms that the particle statistics (both mean and fluctuating) obtained from the SSF model are generally insensitive to whether (19) or (23) is used to sample the gas fluctuating velocity.

In summary, unlike the previous study using the PDFP approach (Shirolkar and McQuay [4]), the particle predictions presented in this study cannot conclusively show any improvements compared to those obtained using eddy lifetime concept. Such observation is not surprising because the particle predictions are strongly dependent on the gas phase predictions. In the previous study the gas turbulence was carefully characterized in the experiments (Snyder and Lumley [5]; Wells and Stock [6]). Thus, it was possible to focus on the differences in the particle dispersion modeling techniques itself. Also, in the previous study the experiments were conducted in a simple flow and hence had the advantage of taking precise, monosized dispersion

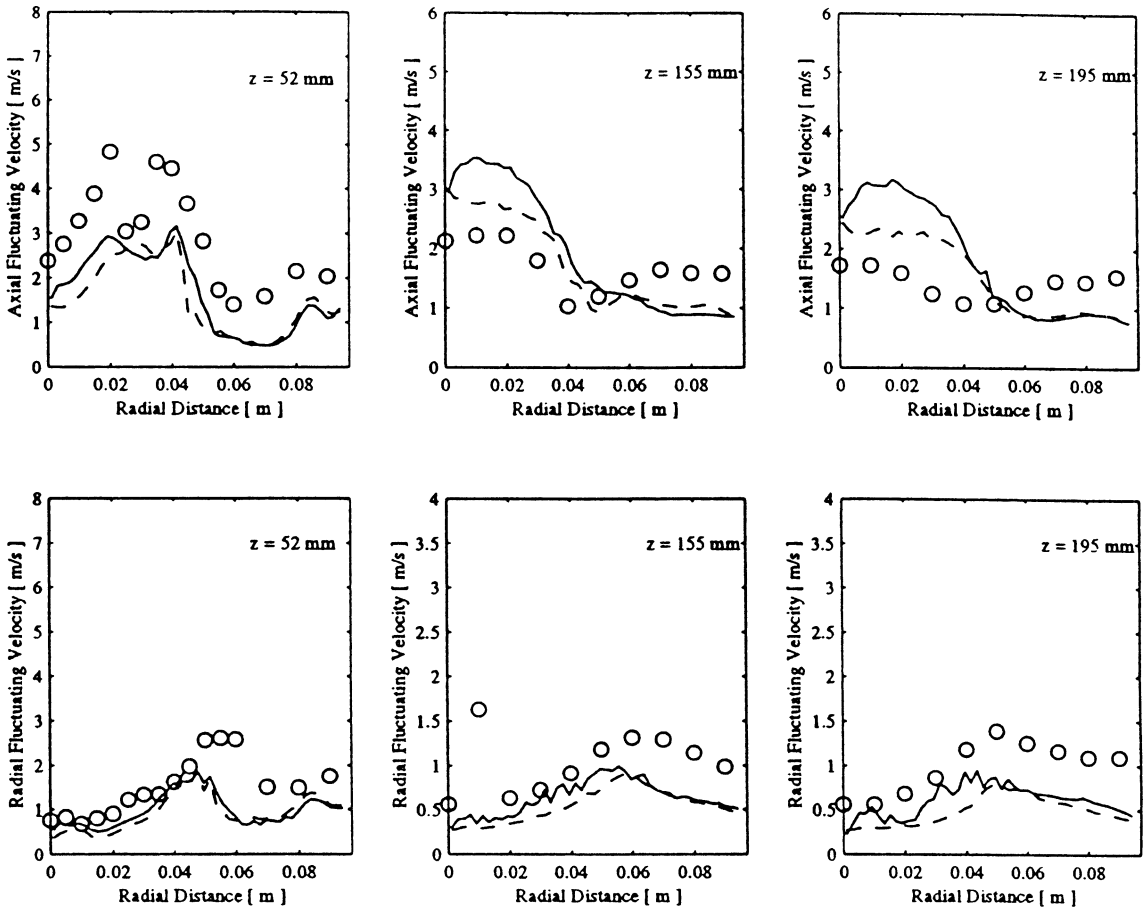

Figure 13. Direct comparison between the experiments and the predictions obtained using the Markov-chain model and the SSF model for the particle axial and radial fluctuating velocities at three different axial locations. Experiment: ○. Simulation: ——, Markov-chain model; – – –, SSF model.

measurements. The flow modeled in this study was complex and the predictions were averaged over the entire size spectrum in order to compare with the available experimental data. In conclusion, the results of this study demonstrate the ability of the PDFP approach to correctly and efficiently model particle dispersion in practical two-phase flows using turbulence models which are applicable to real systems.

4. Concluding remarks

A computationally efficient approach to dispersion modeling that has been successfully demonstrated in turbulent, swirling flows calculates particle ensemble mean trajectories instead of individual particle trajectories. In this model, the particle positional variances are calculated along the mean trajectories, assuming turbulence isotropy. The particle source terms (momentum exchange) are distributed to the carrier phase, which is based on the predicted number particles in a given Eulerian computational cell. This approach has been shown to be more computationally efficient than the standard stochastic dispersion model based on the eddy lifetime concept.

The above technique was validated with the help of the experiments of Sommerfeld and Qiu [29]. The results of the study show that the predictions of both the fluid phase and the particle phase statistics obtained from the present model compared favorably to the experimental data. These predictions were also consistent with those obtained using a stochastic model.

In fluid phase modeling, two different turbulence models were used in this study. The MTS model of Kim and Chen [32] provided better overall predictions for the fluid phase mean velocities compared to the standard k–ε model. Also, the MTS model appeared to better predict the important feature of swirling flows – the central recirculation bubble.

The second-order algebraic relations of Rodi [45] were solved to provide improved estimates for the Reynolds stresses. These estimates are required in the stochastic model to sample the instantaneous fluid velocity vector acting on the particle. The results of the study show that the algebraic relations do provide better estimates for the Reynolds stresses compared to the standard isotropic assumption. However, the results further indicate that the predicted particle statistics are fairly insensitive to differences observed in the Reynolds stresses as predicted by the algebraic relations compared to those obtained assuming turbulence isotropy.

References

[1] Milojevic D., Lagrangian Stochastic-Deterministic (LSD) predictions of particle dispersion in turbulence, Part. Part. Syst. Char. 7 (1990) 181–190.

[2] Lu Q.Q., An approach to modeling particle motion in turbulent flows – I. Homogeneous, isotropic turbulence, Atmos. Environ. 29 (3) (1995) 423–436.

[3] Taylor G.I., Diffusion by continuous movements, P. Lond. Math. Soc. 20 (1921) 196–202.

[4] Shirolkar J.S., McQuay M.Q., Probability density function propagation model for turbulent particle dispersion, Int. J. Multiphase Flow 24 (4) (1998) 663–678.

[5] Snyder W.H., Lumley J.L., Some measurements of particle velocity autocorrelation function in turbulent flow, J. Fluid Mech. 48 (1971) 41–71.

[6] Wells M.R., Stock D.E., The effect of crossing trajectories on the dispersion of particles in a turbulent flow, J. Fluid Mech. 136 (1983) 31–62.

[7] Gosman A.D., Ioannides E., Aspects of computer simulation of liquid-fuelled combustors, presented at the AAIA 19th Aerospace Science Meeting, St Louis, Mo., Paper 81-0323, 1981.

[8] Shuen J.S., Chen L.D., Faeth G.M., Evaluation of a stochastic model of particle dispersion in a turbulent round jet, AIChE J. 29 (1983) 167–170.

[9] Chen P.P., Crowe C.T., On the Monte-Carlo modelling particle dispersion in turbulence, in: Proc. Int. Symp. on Gas–Solid Flows, ASME FED, Vol. 10, 1984, pp. 37–41.

[10] Zhuang Y., Wilson J.D., Lozowski E.P., A trajectory-simulation model for heavy particle motion in turbulent flow, J. Fluids Eng-T ASME 111 (1989) 492–494.

[11] Berlemont A., Desjonqueres P., Gouesbet G., Particle Lagrangian simulation in turbulent flows, Int. J. Multiphase Flow 16 (1) (1990) 19–34.

[12] Burry D., Bergeles G., Dispersion of particles in anisotropic turbulent flows, Int. J. Multiphase Flow 19 (4) (1993) 651–664.

[13] Lu Q.Q., Fontaine J.R., Aubertin G., A Lagrangian model for solid particles in turbulent flows, Int. J. Multiphase Flow 19 (2) (1993) 347–367.

[14] Chen X.-Q., Pereira J.C.F., Predictions of evaporating spray in anisotropically turbulent gas flow, Numer. Heat Tr. A-Appl. 27 (1995) 143–162.

[15] Shirolkar J.S., Coimbra C.F.M., McQuay M.Q., Fundamental aspects of modeling turbulent particle dispersion in dilute flows, Prog. Energy Combust. Sci. 22 (1996) 363–399.

[16] Sawford B.L., Lagrangian statistical simulation of concentration mean and fluctuation fields, J. Climate Appl. Met. 24 (1985) 1152–1166.

[17] Durbin P.A., A stochastic model of two-particle dispersion and concentration fluctuations in homogeneous turbulence, J. Fluid Mech. 100 (1980) 279–302.

[18] Mostafa A.A., Mongia H.C., Evolution of particle-laden jet flows: A theoretical and experimental study, AIAA J. 27 (2) (1989) 167–183.

[19] Adeniji-Fashola A., Chen C.P., Modelling of confined turbulent fluid-particle flows using Eulerian and Lagrangian schemes, Int. J. Heat Mass Tran. 33 (4) (1990) 691–701.

[20] Chen X.-Q., Pereira J.C.F., Efficient Lagrangian stochastic transport modeling of turbulent evaporating sprays, in: 8th Intl. Symp. on Transport Phenomena in Combustion, San Francisco, in press.

[21] Chen X.-Q., Pereira J.C.F., Computation of turbulent evaporating sprays with well-specified measurements: a sensitivity study on droplet properties, Int. J. Heat Mass Trans. 39 (3) (1996) 441–454.

[22] Kohnen G., Ruger M., Sommerfeld M., Convergence behavior for numerical calculations by the Euler/Lagrange method for strongly coupled phases, in: Crowe C.T., Johnson R., Prosperetti A., Sommerfeld M., Tsuji Y. (Eds.), Numerical Methods in Multiphase Flows, ASME FED, Vol. 185, 1994, pp. 191–202.

[23] Berlemont A., Grancher M.S., Gouesbet G., Heat and mass transfer coupling between vaporizing droplets and turbulence using a Lagrangian approach, Int. J. Heat Mass Tran. 38 (16) (1995) 3023–3034.

[24] Coimbra C.F.M., Azevedo J.L.T., Carvalho M.G., 3-D numerical model for predicting NOx emissions from an industrial pulverized coal combustor, Fuel 73 (7) (1994) 1128–1134.
[25] Boyd R.K., Kent J.H., Comparison of large scale boiler data with combustion model predictions, Energy Fuels 8 (1994) 124–130.
[26] Smoot L.D., Smith P.J., Brewster B.S., Baxter L.L., Revised User's Manual: Pulverized Coal Gasification or Combustion – 2 Dimensional, (87-PCGC-2), Brigham Young University, Provo, UT, 1988.
[27] Shirolkar J.S., Queiroz M., Parametric evaluation of a particle dispersion submodel used in a two-dimensional, pulverized-coal combustion code, Energy Fuels 7 (1993) 919–927.
[28] Litchford R.J., Jeng S.M., Efficient statistical transport model for turbulent particle dispersion in sprays, AIAA J. 29 (9) (1991) 1443–1451.
[29] Sommerfeld M., Qiu H.-H., Detailed measurements in a swirling particulate two-phase flow by a phase-Doppler anemometer, Int. J. Heat Fluid Flow 12 (1991) 20–28.
[30] Kim S.W., Calculation of divergent channel flows using a multiple-time-scale turbulence model, AIAA J. 29 (4) (1991) 547–554.
[31] Kim S.W., Chen C.P., A multiple-time-scale turbulence model based on variable partitioning of the turbulent kinetic energy spectrum, NASA CR-179222, 1987.
[32] Kim S.W., Chen C.P., A multiple-time-scale turbulence model based on variable partitioning of the turbulent kinetic energy spectrum, Numer. Heat Tr. B-Fund. 16 (1989) 193–211.
[33] Hayase T., Humphrey J.A.C., Greif R., A consistently formulated QUICK scheme for fast and stable convergence using finite-volume iterative calculation procedures, J. Comput. Phys. 98 (1992) 108–118.
[34] Crowe C.T., Sharma M.P., Stock D.E., The particle-source-in-cell method for gas and droplet flow, J. Fluids Eng-T ASME 99 (1977) 325–332.
[35] Clift R., Grace J.R., Weber M.E., Bubbles, Drops and Particles, Academic Press, New York, 1978.
[36] Smith P.J., Private communication, 1995.
[37] Baxter L.L., Turbulent transport of particles, Ph.D. Dissertation, Brigham Young University, Provo, UT, 1989.
[38] Frenkiel F.N., Etude statistique de la turbulence – fonctions spectrales et coefficients de correlation, Rapport Technique, ONERA No. 34, 1948.
[39] Shirolkar J.S., Modeling Turbulent Particle Dispersion in Dilute, Nonreacting Flows, Ph.D. Dissertation, Brigham Young University, Provo, UT, 1996.
[40] Hanna S.R., Some statistics of Lagrangian and Eulerian wind fluctuations, J. Appl. Meteorol. 18 (1978) 518–528.
[41] Lamb R.G., Hogo H., Reid L.E., A Lagrangian approach to modelling air pollution dispersion – Development and testing in the vicinity of a roadway, US Environmental Protection Agency, EPA-600/4-79-023, 1979.
[42] Reid J.D., Markov chain simulations of vertical dispersion in the neutral surface layer for surface and elevated releases, Bound.-Layer Meteorol. 16 (1979) 3–22.
[43] Azevedo J.L.T., Pereira J.C.F., Calculation of co-axial confined two-phase flows with swirl, in: Sommerfeld M., Wennerberg D. (Eds.), Proceedings of the 5th Workshop on Two Phase Flow Predictions, University of Erlangen, 1990, pp. 199–210.
[44] Sommerfeld M., Ando A., Wennerberg D., Swirling, particle-laden flows through a pipe expansion, J. Fluids Eng-T ASME 144 (1992) 648–655.
[45] Rodi W., Influence of buoyancy and rotation on equations for the turbulent length scale, in: Proceedings of the 2nd Symposium on Turbulent Shear Flows, Imperial College of London, 1979, pp. 10.42–10.47.
[46] Picart A., Berlemont A., Gouesbet G., Modelling and predicting turbulence fields and the dispersion of discrete particles transported by turbulent flows, Int. J. Multiphase Flow 12 (1986) 237–261.
[47] Coimbra C.F.M., Shirolkar J.S., McQuay M.Q., Modeling particle dispersion in a turbulent, incompressible, multiphase mixing layer, J. Wind Eng. Ind. Aerod. 73 (1) (1998) 79–97.
[48] Sommerfeld M., Wennerberg D. (Eds.), Fifth Workshop on Two-Phase Flow Predictions Proceedings, Erlangen, 1990.
[49] Chen C.P., Confined swirling jet predictions using a multiple-scale turbulence model, NASA CR-178484, 1985.
[50] Papoulis A., Probability, Random Variables, and Stochastic Processes, 3rd ed., McGraw-Hill, Inc., 1991.
[51] Litchford R.J., Jeng S.M., Probability density function shape sensitivity in the statistical modeling of turbulent particle dispersion, AIAA J. 30 (10) (1992) 2546–2549.
[52] Ando A., Sommerfeld M., Description of the numerical method for calculation of particle dispersion in a swirling gas-particle flow, in: Sommerfeld M., Wennerberg D. (Eds.), Proceedings of the 5th Workshop on Two Phase Flow Predictions, University of Erlangen, 1990, pp. 34–35.